

# HIGH ORDER CONSERVATIVE SEMI-LAGRANGIAN SCHEME FOR THE BGK MODEL OF THE BOLTZMANN EQUATION

SEBASTIANO BOSCARINO, SEUNG-YEON CHO, GIOVANNI RUSSO, AND SEOK-BAE YUN

**ABSTRACT.** In this paper, we present a conservative semi-Lagrangian finite-difference scheme for the BGK model. Classical semi-Lagrangian finite difference schemes, coupled with an L-stable treatment of the collision term, allow large time steps, for all the range of Knudsen number [12, 22, 25]. Unfortunately, however, such schemes are not conservative. There are two main sources of lack of conservation. First, when using classical continuous Maxwellian, conservation error is negligible only if velocity space is resolved with sufficiently large number of grid points. However, for a small number of grids in velocity space such error is not negligible, because the parameters of the Maxwellian do not coincide with the discrete moments. Secondly, the non-linear reconstruction used to prevent oscillations destroys the translation invariance which is at the basis of the conservation properties of the scheme. As a consequence the schemes show a wrong shock speed in the limit of small Knudsen number. To treat the first problem and ensure machine precision conservation of mass, momentum and energy with a relatively small number of velocity grid points, we replace the continuous Maxwellian with the discrete Maxwellian introduced in [17]. The second problem is treated by implementing a conservative correction procedure based on the flux difference form as in [21]. In this way we can construct a conservative semi-Lagrangian scheme which is Asymptotic Preserving (AP) for the underlying Euler limit, as the Knudsen number vanishes. The effectiveness of the proposed scheme is demonstrated by extensive numerical tests.

## 1. INTRODUCTION

The dynamics of a non-ionized dilute gas at mesoscopic level is described by the celebrated Boltzmann equation [8]. The development of efficient numerical methods for its solution, however, constitutes a formidable challenge, due, among others, to the high dimensionality of the problem, the complicated structure of the collision operator, the need to preserve the collision invariants at a discrete level, and the stiffness issue arising when the Knudsen number is very small.

In view of this situation, Bhatnagar, Gross and Krook, in 1954, suggested a relaxation model of the Boltzmann equation, which now goes by the name of the BGK model [5]. This approximation preserves several important qualitative features of the original Boltzmann equation, such as conservation of mass, momentum and energy, H-theorem and relaxation to equilibrium, and is now widely used as a simplified alternative to the Boltzmann equation because it is much less expensive to treat at a numerical level.

Initial value problem for the BGK model on a periodic domain reads

$$(1.1) \quad \begin{aligned} \frac{\partial f}{\partial t} + v \cdot \nabla_x f &= \frac{1}{\kappa} (\mathcal{M}(f) - f) \\ f(x, v, 0) &= f_0(x, v). \end{aligned}$$

The velocity distribution function  $f(x, v, t)$  represents the mass density of particles at point  $(x, v) \in \mathbb{T}^d \times \mathbb{R}^d$  in phase space, at time  $t > 0$ . The Knudsen number  $\kappa > 0$  is defined as a ratio between the

---

*Key words and phrases.* BGK model, Boltzmann equation, semi-Lagrangian scheme, Conservative correction, Discrete Maxwellian.

G. Russo is partially supported by ITN-ETN Horizon 2020 Project ModCompShock, Modeling and Computation on Shocks and Interfaces, Project Reference 642768. S. Boscarino is supported by the University of Catania (“Piano della Ricerca 2016/2018, Linea di intervento 2”). S.-B. Yun was supported by Samsung Science and Technology Foundation under Project Number SSTF-BA1801-02.

mean free path and a macroscopic characteristic length of the physical system. The local Maxwellian  $\mathcal{M}(f)$  is given by

$$(1.2) \quad \mathcal{M}(f)(x, v, t) := \frac{\rho(x, t)}{\sqrt{(2\pi T(x, t))^d}} \exp\left(-\frac{|v - U(x, t)|^2}{2T}\right),$$

where the macroscopic fields of local density  $\rho(x, t) \in \mathcal{R}^+$ , bulk velocity  $U(x, t) \in \mathbb{R}^d$  and local temperature  $T(x, t) \in \mathbb{R}^+$  are defined through the following relation:

$$(1.3) \quad (\rho(x, t), \rho(x, t)U(x, t), E(x, t)^T) = \langle f\phi(v) \rangle,$$

where

$$\phi(v) = \left(1, v, \frac{1}{2}|v|^2\right)^T, \quad \text{and} \quad \langle g \rangle = \int_{\mathbb{R}^d} g(v) dv.$$

The physical quantity  $E(x, t)$  is the total energy density per unit volume, and it is related to the temperature  $T(x, t)$  by the following relation:

$$E(x, t) = \frac{d}{2}\rho(x, t)T(x, t) + \frac{1}{2}\rho(x, t)|U(x, t)|^2.$$

The BGK model (1.1) satisfies the main properties of the Boltzmann equation such as: conservation of mass, momentum, and energy:

$$(1.4) \quad \langle \mathcal{M}(f)\phi(v) \rangle = \langle f\phi(v) \rangle,$$

as well as entropy dissipation:

$$\int_{\mathbb{R}^d} (\mathcal{M}(f) - f) \ln f dv \leq 0.$$

Note that the equilibrium state clearly is the local Maxwellian determined by  $f$ . Indeed the collision operator vanished for  $f = \mathcal{M}(f)$ . Therefore, the BGK model gives the correct Euler limit as  $\kappa \rightarrow 0$ , i.e., the moments of solution to (1.1), in the limit of vanishing Knudsen number, satisfy the macroscopic compressible Euler equations for a monoatomic gas [4, 6]:

$$(1.5) \quad \begin{aligned} \partial_t \rho + \nabla \cdot (\rho U) &= 0, \\ \partial_t(\rho U) + \nabla \cdot (\rho U \otimes U + pI) &= 0, \\ \partial_t E + \nabla \cdot ((E + p)U) &= 0 \end{aligned}$$

with pressure  $p$  given by the constitutive relation to close the system (1.5)  $p = \rho T$ .

Navier-Stokes equations can be derived by the Chapman-Enskog equation (see for example [9]), by inserting a formal expansion of the distribution function  $f$  in terms of the Knudsen number. To zero-th order one obtains compressible Euler's equations, while to first order in  $\kappa$  one derives the Navier-Stokes equations associated to the BGK model.

We mention that such Navier-Stokes limit is slightly inconsistent with the one obtained from the Boltzmann equation, in that the Prandtl number  $\text{Pr} = c_p \mu / k$  ( $c_p$  is the specific heat at constant pressure,  $\mu$  is the viscosity and  $k$  the thermal conductivity) derived from the BGK model is numerically different from the value computed using the Boltzmann equation. Several techniques have been proposed to overcome this drawback, the most widely adopted being the so-called Ellipsoidal BGK (ES-BGK), see [1, 2, 15]. A semi-Lagrangian method for the ES-BGK model has recently been proposed and analyzed in [24].

The aim of this paper is to develop high order conservative semi-Lagrangian (SL) finite-difference schemes for the BGK model of the Boltzmann equation.

Conservative semi-Lagrangian methods have recently attracted a lot of attention, especially in the context of the Vlasov-Poisson model (see [10, 11]).

General procedures have been developed for the construction of conservative SL schemes, as in [20], however such procedures are often restricted to treat one dimensional problems.

SL schemes for BGK models have recently received increasing interest [12, 22–25] since the SL treatment avoids the classical CFL stability restriction. Furthermore, the implicit treatment of the collision term, which can be easily computed, allows the methods to capture the underlying fluid dynamic limit.

Unfortunately, however, classical SL schemes do not necessarily conserve the total mass, momentum and energy, and the error may become more relevant as the Knudsen number gets smaller [12].

We identify the cause of lack of conservation in the use of continuous Maxwellian in the collision term, and in the non-linear weights adopted in the high order non-oscillatory reconstruction, and propose a remedy based on the use of a discrete Maxwellian (as in [17]) and on a conservative correction to fully restore the conservation properties of the schemes, such as the one adopted in [21] in the case of the Vlasov-Poisson equation.

The paper is organized as follows. Section 2 is devoted to first order schemes. It is shown that the conservation error depends sensitively on the number of velocity grids, and the cause is identified in the use of a continuous Maxwellian in a discrete scheme. We prove that the SL schemes can be made conservative within round-off errors by adopting a discrete Maxwellian in place of the classical continuous one.

Section 3 considers high order SL schemes, which exhibit lack of conservation even with the use of the discrete Maxwellian in the collision term. A conservative correction is then adopted, which restores exact conservation of the methods (within round-off). Section 4 is devoted to linear stability analysis, to explain the stability limitations introduced by the conservative correction. In Section 5 we present several numerical tests, which confirm the expected accuracy and conservation properties of the proposed schemes, and provide numerical evidence of the AP property of the scheme towards the underlying fluid dynamic limit as the Knudsen number vanishes. At the end of we draw some conclusions. The paper deals with 1D case. The extension to the multi-dimensional case is briefly mentioned in the conclusion.

## 2. FIRST ORDER SEMI-LAGRANGIAN SCHEMES

We start from the basic first order semi-Lagrangian scheme [23], and gradually build up to derive our conservative high order semi-Lagrangian scheme (see Section 3).

**2.1. First order SL scheme.** We start from the characteristic formulation of (1.1) :

$$(2.1) \quad \frac{df}{dt} = \frac{1}{\kappa}(\mathcal{M}(f) - f), \quad \frac{dx}{dt} = v,$$

subject to the initial data:  $f(x, v, 0) = f_0(x, v)$ .

We consider one dimensional problem in space and velocity, and we divide the spatial and velocity domain into uniform grids with mesh spacing  $\Delta x$  and  $\Delta v$ , respectively. We also use uniform time step  $\Delta t$ . Given an computational domain,  $[x_{min}, x_{max}] \times [v_{min}, v_{max}] \times [0, T^f]$ , we denote the grid points by

$$\begin{aligned} x_i &= x_{min} + (i - \frac{1}{2})\Delta x, & (i = 1, \dots, N_x) \\ v_j &= v_{min} + j\Delta v, & (j = 0, \dots, N_v) \\ t^n &= n\Delta t, & (n = 0, \dots, N_t), \end{aligned}$$

where  $N_x$ ,  $N_v + 1$  and  $N_t$  are the number of grid nodes in space, velocity and time, respectively, so that  $x_{max} = x_{min} + N_x\Delta x$ ,  $v_{max} = v_{min} + N_v\Delta v$  and  $T^f = N_t\Delta t$ .

Let  $f_{i,j}^n$  denote a discrete approximation of  $f(x_i, v_j, t^n)$  and  $\phi(v_j) = \left(1, v_j, \frac{v_j^2}{2}\right)^T$ . Applying first order semi-Lagrangian implicit Euler (IE-SL) scheme to (2.1), we get

$$(2.2) \quad f_{i,j}^{n+1} = \tilde{f}_{ij}^n + \frac{\Delta t}{\kappa} (\mathcal{M}(f_{i,j}^{n+1}) - f_{i,j}^n),$$

where  $\tilde{f}_{ij}^n$  is an approximation of  $f(x_i - v_j \Delta t, v_j, n \Delta t)$  obtained by a suitable interpolation from  $\{f_{ij}^n\}$ . Note that linear reconstruction will be sufficient for first order SL scheme, while a higher order non-oscillatory reconstruction is necessary for high order accuracy. The Maxwellian  $\mathcal{M}(f_{i,j}^{n+1})$  is given by

$$(2.3) \quad \mathcal{M}(f_{i,j}^{n+1}) = \frac{\rho_i^{n+1}}{\sqrt{2\pi T_i^{n+1}}} \exp\left(-\frac{|v_j - U_i^{n+1}|^2}{2T_i^{n+1}}\right),$$

where discrete macroscopic moments are constructed from  $f^{n+1}$  as follows:

$$\begin{pmatrix} \rho_i^{n+1} \\ \rho_i^{n+1} U_i^{n+1} \\ E_i^{n+1} \end{pmatrix} = \sum_{j=0}^{N_v} f_{i,j}^{n+1} \phi(v_j) \Delta v,$$

which is equivalent to using midpoint rule in the computation of the momentums, Eq. (1.3).

We now employ a technique that enables one to explicitly solve the implicit scheme (2.2). For this, we multiply both sides in (2.2) by  $\phi(v_j)$ , sum over  $j$ , and use the property that the moments of  $\mathcal{M}(f_{i,j}^{n+1}) - f_{i,j}^{n+1}$  up to second order vanish, to obtain

$$\sum_j^{N_v+1} f_{i,j}^{n+1} \phi(v_j) \Delta v = \sum_j^{N_v+1} \tilde{f}_{ij}^n \phi(v_j) \Delta v.$$

This gives

$$\begin{pmatrix} \rho_i^{n+1} \\ U_i^{n+1} \\ E_i^{n+1} \end{pmatrix} = \begin{pmatrix} \tilde{\rho}_i^n \\ \tilde{U}_i^n \\ \tilde{E}_i^n \end{pmatrix},$$

with

$$\begin{pmatrix} \tilde{\rho}_i^n \\ \tilde{\rho}_i^n \tilde{U}_i^n \\ \tilde{E}_i^n \end{pmatrix} = \sum_{j=0}^{N_v} \tilde{f}_{ij}^n \phi(v_j) \Delta v, \quad \tilde{E}_i^n = \frac{1}{2} \tilde{\rho}_i^n |\tilde{U}_i^n|^2 + \frac{1}{2} \tilde{\rho}_i^n \tilde{T}_i^n.$$

Therefore, we can legitimately replace  $\mathcal{M}(f_{i,j}^{n+1})$  with  $\mathcal{M}(\tilde{f}_{ij}^n)$ , so that the scheme becomes

$$f_{i,j}^{n+1} = \tilde{f}_{ij}^n + \frac{\Delta t}{\kappa} \left( \mathcal{M}(\tilde{f}_{ij}^n) - f_{i,j}^{n+1} \right),$$

which gives

$$(2.4) \quad f_{i,j}^{n+1} = \frac{\kappa \tilde{f}_{ij}^n + \Delta t \mathcal{M}(\tilde{f}_{ij}^n)}{\kappa + \Delta t}.$$

This approach has been fruitfully used, for example, in [12, 19, 22, 23]. Note that scheme (2.4) allows us to use large  $\text{CFL} > 1$  numbers.

Summarizing, we have the following procedure (see Fig.1):

- (1) Use linear interpolation to obtain  $\tilde{f}_{ij}^n$  from  $\{f_{ij}^n\}$ .
- (2) Compute  $\mathcal{M}(\tilde{f}_{ij}^n)$  from  $\{\tilde{f}_{ij}^n\}$  by using the approximate macroscopic moments, i.e.  $(\tilde{\rho}_i^n, \tilde{U}_i^n, \tilde{E}_i^n)^T$ .
- (3) Compute numerical solution using (2.4).

We apply the scheme to the propagation of a single shock, where we can compare the numerical solution to the exact one, and therefore accurately check the conservation properties of the scheme.

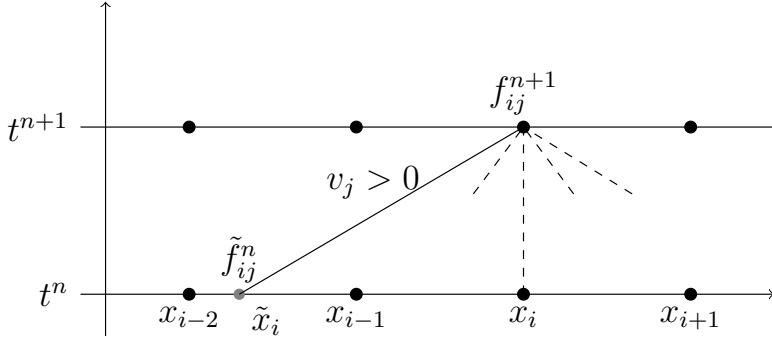


FIGURE 1. Representation of the implicit first order scheme.

**2.2. Test 1.** We apply IE-SL scheme (2.4) to equation (1.1) with  $f_0$  given by the Maxwellian w.r.t macroscopic quantities

$$(\rho_0, u_0, p_0) = \begin{cases} \left( \frac{(\gamma+1)M^2}{(\gamma-1)M^2+2}, \frac{2\sqrt{\gamma}(M^2-1)}{(\gamma+1)M}, 1 + \frac{2\gamma(M^2-1)}{(\gamma+1)} \right), & \text{for } x \leq 0.5 \\ (1, 0, 1), & \text{for } x > 0.5. \end{cases}$$

We take the Knudsen number  $\kappa = 10^{-6}$ , the polytropic constant  $\gamma = 3$  (corresponding to a polytropic gas with one degree of freedom per gas molecule) and Mach number  $M = 2$ .

To prevent the solution from reaching the boundary, final time is taken  $T_f = 0.4$ . We used free flow boundary conditions and performed the computation on  $(x, v) \in [0, 5] \times [-20, 20]$ .

The results are summarized in Table 1, where the conservation errors are reported for various values of  $N_x$  and  $N_v$ .

$N_v$	IE-SL-Linear-CM, $N_x = 100$			IE-SL-Linear-CM, $N_x = 200$		
	Mass	Momentum	Energy	Mass	Momentum	Energy
30	3.63e-04	0.0012	0.0021	9.10e-04	0.0030	0.0051
40	5.54e-08	3.26e-07	6.03e-07	1.15e-07	6.43e-07	1.25e-06
50	8.55e-13	7.81e-12	1.43e-11	1.78e-12	1.54e-11	2.97e-11
60	3.55e-14	4.96e-14	3.89e-14	7.45e-14	8.24e-14	7.23e-14
90	3.24e-14	4.82e-14	3.77e-14	7.16e-14	7.32e-14	7.45e-14

TABLE 1.  $CFL = 4$ ,  $\kappa = 10^{-6}$ . First order scheme, conservation error of discrete moments in relative  $L_1$  norm for single shock with velocity domain  $[-20, 20]$ .

From the results we can make the following observations:

- (1) Table 1 shows that the first order IE-SL scheme with enough points in velocity space maintains conservation within machine precision, independently of the number of grid point in space;
- (2) the same scheme with smaller number of points in velocity produces non-negligible conservation errors.

This numerical evidence suggests that the convection part is conservative, while errors in conservation are a consequence of the numerical approximation of the relaxation term. The lack of conservation is indeed due to the use of a continuous Maxwellian on a discrete scheme in velocity: the parameters of the continuous Maxwellian do not coincide with the discrete moments, they are just approximated by them with spectral accuracy when the integrals are replaced by a summation. The spectral accuracy of the quadrature explains, for example, the dramatic drop of the conservation error when the number of points in velocity is increased from 40 to 50.

**2.3. Classical SL scheme with the discrete Maxwellian.** In this section, we replace the continuous Maxwellian with the discrete Maxwellian to resolve the problem of strong dependence of the conservation error on the number of velocity grids.

**2.3.1. Discrete Maxwellian.** We start by briefly describing the discrete Maxwellian introduced in [17]. In that work, the author proved that a discrete entropy minimization problem has a uniqueness solution called the discrete Maxwellian( $d\mathcal{M}$ ). Moreover, together with an assumption that if a set of discrete velocity points  $\{v_j\}$  is rank  $d+2$ , there exist a unique vector  $a(x, t) \in \mathbb{R}^{d+2}$  such that the following exponential characterization holds:

$$(2.5) \quad d\mathcal{M}(x, v_j, t) := \exp(a(x, t) \cdot \phi(v_j)),$$

if and only if there exists a set of  $\{g_j > 0\}_j$  such that

$$\sum_j f(x, v_j, t) \phi(v_j) (\Delta v)^d = \sum_j g_j \phi(v_j) (\Delta v)^d$$

where  $f(x, v_j, t)$  are given. The vector  $a(x, t)$  is determined by solving the following non-linear system:

$$(2.6) \quad \sum_{j=0}^{N_v} f(x, v_j, t) \phi(v_j) \Delta v = \sum_{j=0}^{N_v} \exp(a(x, t) \cdot \phi(v_j)) \phi(v_j) \Delta v.$$

In practice, employing a Newton algorithm, we find  $a(x, t)$  such that

$$(2.7) \quad \max_{1 \leq \ell \leq 3} \left| \sum_{j=0}^{N_v} (f(x, v_j, t) - d\mathcal{M}(x, v_j, t)) \phi_\ell(v_j) \Delta v \right| < tol$$

for arbitrary small tolerance( $tol$ ). Throughout this paper, we take  $tol$  to be the order of  $10^{-14}$ . Here, we denote the  $\ell$ th component of  $\phi(v_j)$  by  $\phi_\ell(v_j)$ ,  $\ell = 1, 2, 3$ . With the use of discrete Maxwellian in (2.4),

$$(2.8) \quad f_{i,j}^{n+1} = \frac{\kappa \tilde{f}_{ij}^n + \Delta t d\mathcal{M}(\tilde{f}_{ij}^n)}{\kappa + \Delta t},$$

and it is possible to prove the following estimate on the conservation error (see Appendix A):

$$\max_{1 \leq \ell \leq 3} \left| \sum_{i=1}^{N_x} \sum_{j=0}^{N_v} (f_{i,j}^{Nt} - f_{i,j}^0) \phi_\ell(v_j) \Delta v \Delta x \right| \leq \frac{N_t \Delta t}{\kappa + \Delta t} (x_{max} - x_{min}) tol.$$

On the other hand, we recall that, in discrete velocity models, we need to take the velocity domain sufficiently large to secure correct profile of macroscopic moments, especially when there is a large space variation of mean velocity  $U$  and temperature  $T$ .

Therefore, it is necessary to balance the size of the velocity domain needed for the accurate computation of macroscopic fields, and the efficient choice of smallest possible number of grids to guarantee the efficient performance of the scheme. (See Test 2 in Section 5.)

Such issues of the optimal choice of the grid points in velocity space is not considered here and will be left for future investigation.

### 3. HIGH ORDER SCHEMES AND CONSERVATIVE CORRECTION

Several techniques can be adopted to obtain high order accuracy and to ensure the shock capturing properties near the fluid regime, avoiding spurious oscillations. Here we consider two of the schemes adopted in [12], namely third order schemes obtained by combining high order methods in time (RK3 and BDF3) with a high order non-oscillatory spatial interpolation technique that we call generalized WENO (G-WENO) [7] to obtain high order accuracy and to ensure the shock capturing properties of the proposed schemes near the fluid regime, avoiding spurious oscillations (see the Section 5).

We repeat the same moving shock test using third order schemes, and the results are summarized in Table 2 for SL schemes using Runge-Kutta time advancement (RK3-W35), and in Table 3 for the

$(N_x, N_v)$	Classical RK3-W35-CM			Classical RK3-W35-DM		
	Mass	Momentum	Energy	Mass	Momentum	Energy
(100, 42)	1.28e-03	1.25e-02	1.40e-01	1.22e-03	1.29e-02	1.47e-02
(100, 50)	1.06e-03	1.31e-02	1.47e-02	1.06e-03	1.36e-02	1.47e-02
(100, 60)	1.43e-03	1.26e-02	1.49e-02	1.43e-03	1.26e-02	1.49e-02
(100, 90)	1.35e-03	1.28e-02	1.48e-02	1.35e-03	1.28e-02	1.48e-02
(200, 42)	1.54e-03	1.30e-02	1.45e-02	1.48e-03	1.33e-02	1.52e-02
(200, 50)	1.30e-03	1.35e-02	1.51e-02	1.30e-03	1.35e-02	1.51e-02
(200, 60)	1.68e-03	1.30e-02	1.53e-02	1.68e-03	1.30e-02	1.53e-02
(200, 90)	1.60e-03	1.32e-02	1.53e-02	1.60e-03	1.32e-02	1.53e-02
(400, 42)	1.68e-03	1.32e-02	1.47e-02	1.61e-03	1.35e-02	1.54e-02
(400, 50)	1.42e-03	1.36e-02	1.53e-02	1.42e-03	1.36e-02	1.53e-02
(400, 60)	1.80e-03	1.32e-02	1.55e-02	1.80e-03	1.32e-02	1.55e-02
(400, 90)	1.73e-03	1.34e-02	1.54e-02	1.73e-03	1.34e-02	1.54e-02
(800, 60)	1.86e-03	1.33e-02	1.55e-02	1.86e-03	1.33e-02	1.55e-02
(800, 90)	1.80e-03	1.34e-02	1.55e-02	1.80e-03	1.34e-02	1.55e-02

TABLE 2.  $CFL = 2$ ,  $\kappa = 10^{-6}$ . High order schemes, conservation error of discrete moments in relative  $L_1$  norm for single shock problem with velocity domain  $[-20, 20]$ .

BDF-based SL schemes (BDF3-W35). Fully resolved high order schemes both in space and velocity produce finite conservation error, which is much larger than the conservation error of the first order scheme, shown in Table 1.

This indicates that there are cases where high order schemes may show even bigger conservation errors compared to those obtained by the first order scheme.

The main qualitative difference between first order and high order methods is that the former uses a fixed stencil for the linear interpolation at the foot of the characteristics, while high order non-oscillatory reconstructions such as G-WENO use a weighted sum of reconstructions on different stencils, the weight depending on the local regularity properties of the function to be reconstructed. As a result, in the first order SL scheme the interpolation weights are the same for all intervals, whereas in high order SL schemes, due to the nonlinearity of the non-oscillatory reconstruction, the interpolation weights are not the same for all intervals, thus destroying the translation invariance which is at the basis of the conservation property of the schemes.

**3.1. Conservative correction and discrete Maxwellian.** In subsection 2.3, we achieved a machine precision conservation error for first order scheme by implementing the discrete Maxwellian in place of the continuous one. This remedy, however, is not sufficient in high order implementations, as was indicated in Table 2, 3.

To overcome this, we modify the scheme (2.8) using the conservative correction procedure based on a flux difference form [18, 21] to derive our main scheme.

For clarity of exposition, we start by describing the procedure in the case of first order schemes, although its real benefit appears in its application to high order methods.

The conservative method can be viewed as a predictor-corrector method. It is based on a SL non-conservative prediction, and a conservative correction.

With reference to Figure 2, the first order scheme with conservative correction works as follows:

- (1) using (2.8), predict  $f_{i,j}^{(1)}$  from  $\{f_{i,j}^n\}$  at time  $t^{n+1}$ ;
- (2) reconstruct  $\widehat{F}_{i+\frac{1}{2},j}^{(1)}$  and  $\widehat{F}_{i-\frac{1}{2},j}^{(1)}$  from  $\{v_j f_{i,j}^{(1)}\}$ , by using a suitable high order reconstruction (see Sect. 3.2);

$(N_x, N_v)$	Classical BDF3-W35-CM			Classical BDF3-W35-DM		
	Mass	Momentum	Energy	Mass	Momentum	Energy
(100, 42)	1.73e-03	1.03e-02	1.39e-02	1.72e-03	1.03e-02	1.39e-02
(100, 50)	1.58e-03	1.04e-02	1.38e-02	1.58e-03	1.04e-02	1.38e-02
(100, 60)	1.73e-03	1.00e-02	1.38e-02	1.73e-03	1.00e-02	1.38e-02
(100, 90)	1.75e-03	1.03e-02	1.40e-02	1.75e-03	1.03e-02	1.40e-02
(200, 42)	2.02e-03	1.10e-02	1.46e-02	2.01e-03	1.10e-02	1.46e-02
(200, 50)	1.88e-03	1.11e-02	1.45e-02	1.88e-03	1.11e-02	1.45e-02
(200, 60)	2.01e-03	1.07e-02	1.44e-02	2.01e-03	1.07e-02	1.44e-02
(200, 90)	2.03e-03	1.10e-02	1.46e-02	2.03e-03	1.10e-02	1.46e-02
(400, 42)	2.18e-03	1.14e-02	1.49e-02	2.18e-03	1.14e-02	1.49e-02
(400, 50)	2.05e-03	1.15e-02	1.48e-02	2.05e-03	1.15e-02	1.48e-02
(400, 60)	2.16e-03	1.11e-02	1.47e-02	2.16e-03	1.11e-02	1.47e-02
(400, 90)	2.19e-03	1.14e-02	1.49e-02	2.19e-03	1.14e-02	1.49e-02
(800, 60)	2.24e-03	1.13e-02	1.49e-02	2.24e-03	1.13e-02	1.49e-02
(800, 90)	2.27e-03	1.16e-02	1.51e-02	2.27e-03	1.16e-02	1.51e-02

TABLE 3.  $CFL = 2$ ,  $\kappa = 10^{-6}$ . High order schemes, conservation error of discrete moments in relative  $L_1$  norm for single shock problem with velocity domain  $[-20, 20]$ .

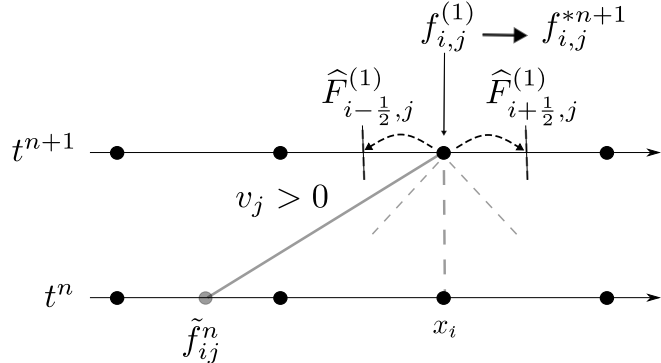


FIGURE 2. Representation of first order scheme with conservative correction.

(3) compute the convective term  $f_{i,j}^{*n+1}$  by the conservative scheme

$$f_{i,j}^{*n+1} = f_{i,j}^n - \frac{\Delta t}{\Delta x} (\hat{F}_{i+\frac{1}{2},j}^{(1)} - \hat{F}_{i-\frac{1}{2},j}^{(1)});$$

(4) compute the discrete Maxwellian  $dM_{i,j}^{*n+1}$  from  $f_{i,j}^{*n+1}$ ;

(5) update the solution  $f_{i,j}^{n+1}$  using

$$(3.1) \quad f_{i,j}^{n+1} = f_{i,j}^{*n+1} + \frac{\Delta t}{\kappa} (dM_{i,j}^{*n+1} - f_{i,j}^{n+1})$$

Here  $\hat{F}$  is an accurate reconstruction of the flux  $vf$  in the sense of conservative finite difference [26]. We only present the formulation in 1D. Extension to more dimensions can be obtained performing a dimension by dimension 1D reconstruction of the fluxes.

*Remark 3.1.* The conservative correction imposes severe stability restriction on the CFL number for the C-SL schemes (for a theoretical investigation see [21]). An accurate analysis for high order Runge-Kutta or BDF C-SL schemes will be given in Sect.5.

**3.2. Spatial discretization.** We restrict ourselves to 1D case and adopt a uniform grid  $\Delta x := x_{i+1} - x_i$ .

*Flux computation at the foot of the characteristics.* We use the Generalized WENO reconstruction (G-WENO) introduced in [7] for non-oscillatory high-order reconstruction of  $\tilde{f}_{ij}^n$ . The main advantage of such a reconstruction is its use of polynomial weights, which provide a general framework to implement WENO interpolation on any points in a cell. See Appendix B for details.

In our C-SL scheme, we need an accurate approximation of the convection term:  $v\partial_x f$ . For this, we set  $F(f) := vf$ , and look for a function  $\hat{F}$  such that

$$(3.2) \quad F_i = \frac{1}{\Delta x} \int_{x_{i-\frac{1}{2}}}^{x_{i+\frac{1}{2}}} \hat{F} dx.$$

where  $F_i = F(f(x_i, v, t))$ . Then we can compute the convection term using the following relation:

$$(3.3) \quad \partial_x F_i = \frac{1}{\Delta x} \left( \hat{F}(x_{i+\frac{1}{2}}) - \hat{F}(x_{i-\frac{1}{2}}) \right).$$

To compute  $\hat{F}(x_{i\pm\frac{1}{2}})$ , we use the classical WENO reconstruction in [26] to guarantee non-oscillatory high-order approximation of  $\hat{F}_{i\pm\frac{1}{2}}$ . In this reconstruction, we actually find a piecewise polynomial function that interpolates  $\{F_i\}_{i=1\dots N_x}$ . Since those polynomials contain discontinuity at cell boundaries  $x_{i\pm\frac{1}{2}}$ , it is necessary to pick the correct direction where information comes from. For this reason, upwinding is introduced by flux splitting:

$$F = F^+ + F^-$$

where

$$F^+(f) = \begin{cases} vf, & v > 0 \\ 0, & \text{otherwise} \end{cases}, \quad F^-(f) = \begin{cases} 0, & v > 0 \\ vf, & \text{otherwise} \end{cases},$$

so that (3.2) can be rewritten as  $F_i = F_i^+ + F_i^-$ , where

$$F^\pm(x) = \frac{1}{\Delta x} \int_{x-\Delta x/2}^{x+\Delta x/2} \hat{F}^\pm(\xi) d\xi.$$

The half fluxes  $\hat{F}^\pm(x)$  are obtained by piecewise polynomial reconstruction:

$$\hat{F}^\pm(x) = \sum_i \chi_i(x) \hat{F}_i^\pm(x)$$

where  $\chi_i(x)$  denotes the characteristic function of interval  $[x_{i-1/2}, x_{i+1/2}]$ .

Then, by standard WENO process [26], we reconstruct  $\hat{F}_i^\pm(x)$  from  $\{F_i^\pm\}$ . Finally, our numerical flux is obtained as follows:

$$\hat{F}_{i+\frac{1}{2}} = \hat{F}_i^+(x_{i+1/2}) + \hat{F}_{i+1}^-(x_{i+1/2}).$$

**3.3. Time discretization.** High order discretization in time can be obtained by Runge-Kutta methods (RK) or backward differentiation formulas (BDF) [14]. For the sake of simplicity, we again consider the one-dimensional problem in space and velocity with uniform grid in time.

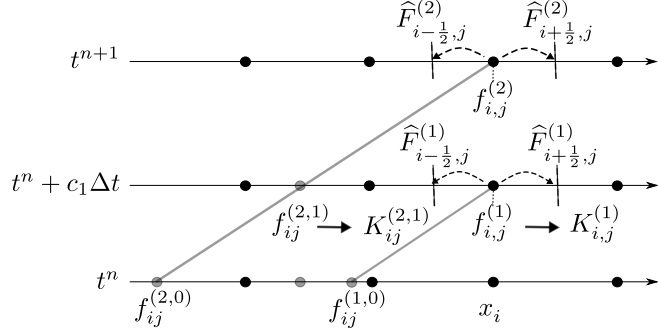


FIGURE 3. Representation of DIRK2 scheme with conservative correction.

*Runge-Kutta methods.* Our system (2.1) becomes *stiff* as  $\kappa \rightarrow \infty$ . To overcome this difficulty, we need stable schemes. In view of this, *L-stable diagonally implicit Runge-Kutta* (DIRK) methods provide a balanced performance between stability and efficiency [13].

DIRK methods can be represented using the Butcher's table

$$(3.4) \quad \begin{array}{c|c} c & A \\ \hline & b^T \end{array}$$

where  $A = (a_{kl})$  is a  $s \times s$  lower triangle matrix and  $c = (c_1, \dots, c_s)^T$  and  $b = (b_1, \dots, b_s)^T$  are coefficients vectors [14].

In order to guarantee *L*-stability, here we make use of *stiffly accurate* schemes (SA), i.e. schemes for which the last row of matrix  $A$  is equal to the vector of weights:  $a_{s,j} = b_j, j = 1, \dots, s$ . This will ensure that the absolute stability function vanishes at infinity. As a consequence, an  $A$ -stable scheme which is SA is also *L*-stable [13].

Now, we illustrate our *L*-stable DIRK schemes to approximate the characteristic system (2.1) coupled with the conservative correction and the discrete Maxwellian. In the following,  $f_{ij}^{(k,\ell)}$ ,  $\ell = 0, \dots, s$ , denotes the  $\ell$ -th stage value computed along the  $k$ -th characteristic corresponding to each  $x_i$  and  $v_j$ , see Figures 3. For example, in the case of  $\ell = 0$ ,  $f_{ij}^{(k,0)}$  is the approximation of  $f(x_i - c_k \Delta t v_j, v_j, t^n)$  reconstructed from  $\{f_{i,j}^n\}$ . We also define the RK flux  $K_{ij}^{(k,\ell)}$  by

$$K_{ij}^{(k,\ell)} = \frac{1}{\kappa} (d\mathcal{M}_{ij}^{(k,\ell)} - f_{ij}^{(k,\ell)}), \quad \ell = 1, \dots, s.$$

3.3.1. *Algorithm DIRK.* For  $k = 1, \dots, s$ .

- *Non-conservative step*
  - (1) Compute  $f_{ij}^{(k,0)}$  in  $x_{ij}^{(k,0)} := x_i - c_k v_j \Delta t$  along the  $k$ -th characteristic by interpolation from  $\{f_{i,j}^n\}$ .
  - (2) Compute:

$$f_{ij}^{(k)} = f_{ij}^{(k,0)} + \Delta t \sum_{\ell=1}^{k-1} a_{k\ell} K_{ij}^{(k,\ell)} + \frac{\Delta t}{\kappa} a_{kk} (d\mathcal{M}_{ij}^{(k)} - f_{ij}^{(k)})$$

where  $d\mathcal{M}_{ij}^{(k)}$  is computed imposing, within some tolerance, that

$$(3.5) \quad \sum_j \phi_j d\mathcal{M}_{ij}^{(k)} \Delta v = \sum_j \phi_j (f_{ij}^{(k,0)} + \Delta t \sum_{\ell=1}^{k-1} a_{k\ell} K_{ij}^{(k,\ell)}) \Delta v, \quad \phi_j = 1, v_j, v_j^2/2.$$

(3) Compute:

$$K_{i,j}^{(k)} = \frac{1}{\kappa} \left( d\mathcal{M}_{i,j}^{(k)} - f_{i,j}^{(k)} \right).$$

(4) Compute the RK flux  $K_{i,j}^{(\ell,k)}$  in  $x_{ij}^{(\ell,k)} := x_i - (c_\ell - c_k)v_j\Delta t$  with  $\ell = k+1, \dots, s$  along the  $\ell$ -th characteristic by interpolation from  $\{K_{i,j}^{(k)}\}$ .

(5) Reconstruct  $\widehat{F}_{i+1/2,j}^{(k)}$  from  $\{v_j f_{i,j}^{(k)}\}$  using G-WENO reconstruction [26] within a *finite difference formulation* (fd).

- *Conservative correction step*

(1) Compute the conservative convection:

$$f_{i,j}^* = f_{i,j}^n + \frac{\Delta t}{\Delta x} \sum_{\ell=1}^s b_\ell \left( \widehat{F}_{i+1/2,j}^{(\ell)} - \widehat{F}_{i-1/2,j}^{(\ell)} \right).$$

(2) Compute conservative solution:

$$f_{i,j}^{n+1} = f_{i,j}^* + \Delta t \sum_{\ell=1}^{s-1} b_\ell K_{i,j}^{(\ell)} + \frac{\Delta t}{\kappa} b_s \left( d\mathcal{M}_{i,j}^{(*)} - f_{i,j}^{n+1} \right)$$

where  $d\mathcal{M}_{i,j}^{(*)}$  is computed imposing, within some tolerance, that

$$(3.6) \quad \sum_j \phi_j d\mathcal{M}_{i,j}^{(*)} \Delta v = \sum_j \phi_j f_{i,j}^* \Delta v, \quad \phi_j = 1, v_j, v_j^2/2.$$

In the previous expression, the terms containing  $K_{i,j}^{(\ell)}$  vanish because the intermediate Maxwellians have the same moments of the stage values.

*BDF methods.* Another time discretization we use for the stable approximation of stiff problems (2.1) is the backward differentiation formula (BDF) (see [13]) whose general form is given by

$$BDF : y^{n+1} = \sum_{k=1}^s a_k y^{n+1-k} + \beta_s \Delta t g(y^{n+1}, t_{n+1})$$

with  $\beta_s \neq 0$ . For our work, we use BDF2 and BDF3:

$$(3.7) \quad \begin{aligned} BDF2 : y^{n+1} &= \frac{4}{3}y^n - \frac{1}{3}y^{n-1} + \frac{2}{3}\Delta t g(y^{n+1}, t_{n+1}), \\ BDF3 : y^{n+1} &= \frac{18}{11}y^n - \frac{9}{11}y^{n-1} + \frac{2}{11}y^{n-2} + \frac{6}{11}\Delta t g(y^{n+1}, t_{n+1}). \end{aligned}$$

BDF schemes have some advantages over DIRK since a smaller number of numerical determination of the discrete Maxwellian and fluxes are needed and fewer interpolations are required. For BDF2 and BDF3, there is only one stage in which we have to compute the discrete Maxwellian and fluxes while two and three stages are required for DIRK2 and DIRK3 schemes respectively. Moreover, BDF2 and BDF3 schemes require two and three steps for interpolations whereas DIRK2 and DIRK3 schemes require three and six steps respectively. The price to pay is that BDF has more severe stability restriction than DIRK (See Section 5).

**3.3.2. Algorithm BDF.** Let  $a_k$ , and  $\beta_s$  be the coefficients of a BDF method of order  $s$ . Given a discrete approximation  $\{f_{ij}^n\}$  of the distribution function at time  $t_n$ ,  $\{f_{ij}^{n+1}\}$  is computed by the following steps

- *Non-conservative step.*

(1) For  $k = 1, \dots, s$ , interpolate  $f_{ij}^{n,k} = f(x_i - kv_j\Delta t, v_j, t^{n+1-k})$  in  $x_{ij}^k := x_i - kv_j\Delta t$  from  $\{f_{ij}^{n+1-k}\}$  with a suitable *generalized* WENO reconstruction in [7].

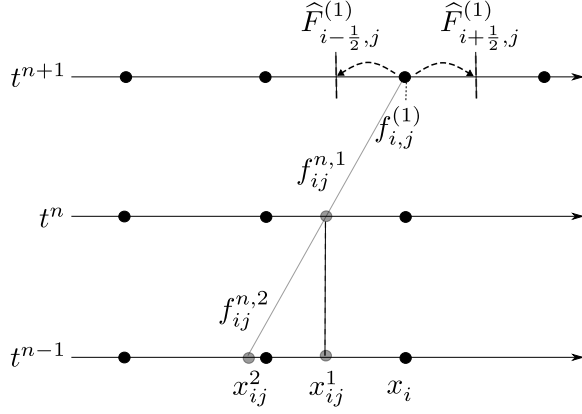


FIGURE 4. Representation of BDF2 scheme with conservative correction. Black circles: grid nodes, grey circles: points where interpolation is needed.

(2) Compute  $f_{i,j}^* = \sum_{k=1}^s a_k f_{ij}^{n,k}$  and

$$f_{i,j}^{(1)} = f_{i,j}^* + \beta_s \frac{\Delta t}{\kappa} \left( d\mathcal{M}_{i,j}^{(1)} - f_{i,j}^{(1)} \right)$$

where  $d\mathcal{M}_{i,j}^{(1)}$  is computed imposing, within some tolerance, that

$$(3.8) \quad \sum_j \phi_j d\mathcal{M}_{i,j}^{(1)} \Delta v = \sum_j \phi_j f_{i,j}^* \Delta v, \quad \phi_j = 1, v_j, v_j^2/2.$$

- *Conservative correction step*

- (1) Reconstruct  $\hat{F}_{i+1/2,j}^{(1)}$  from  $\{v_j f_{i,j}^{(1)}\}$  using WENO reconstruction in the framework of the *conservative finite difference formulation* (fd) [26].
- (2) Conservative convection:  $f_{i,j}^{**} = \sum_{k=1}^s a_k f_{i,j}^{n+1-k} - \beta_s \frac{\Delta t}{\Delta x} \left( \hat{F}_{i+1/2,j}^{(1)} - \hat{F}_{i-1/2,j}^{(1)} \right)$ .
- (3) Compute conservative solution:

$$f_{i,j}^{n+1} = f_{i,j}^{**} + \beta_s \frac{\Delta t}{\kappa} \left( d\mathcal{M}_{i,j}^{n+1} - f_{i,j}^{n+1} \right).$$

Note that  $d\mathcal{M}_{i,j}^{n+1} = d\mathcal{M}(f_{i,j}^{**})$  as in (3.8).

Schematics of BDF2 is illustrated in Fig. 4.

The conservative correction imposes some stability restrictions on the time step. The next section is devoted to the stability analysis of RK and BDF schemes applied to the linear advection equation.

#### 4. LINEAR STABILITY ANALYSIS

In this section we perform the stability analysis of conservative semi-Lagrangian scheme for the 1D advection equation. Following [21] we consider the linear transport equation

$$(4.1) \quad u_t + vu_x = 0, \quad u(x, 0) = u_0(x), \quad v \in \mathbb{R}.$$

For simplicity, we assume a periodic boundary condition and  $x \in [-\pi, \pi]$ .

Algorithm 3.3.1 applied to (4.1) gives

$$(4.2) \quad u_j^{n+1} = u_j^n - \frac{\Delta t}{\Delta x} \sum_{\ell=1}^s b_\ell v \left( \hat{u}_{j+1/2}^{(\ell)} - \hat{u}_{j-1/2}^{(\ell)} \right),$$

where  $\hat{u}_{j+1/2}^{(\ell)}$  are obtained from the stage values  $u_j^{(\ell)} = u^n(x_j - vc_\ell \Delta t)$  by reconstruction, and  $u^n(x)$  denotes a suitable interpolation from  $\{u_j^n\}$ .

4.1. **Fourier interpolation.** We look for the evolution of a Fourier mode of the form

$$u_j^n = \rho^n e^{ikj\Delta x} = \rho^n e^{ij\xi}, \quad \xi = k\Delta x, \quad i = \sqrt{-1}.$$

In the analysis we first consider Fourier interpolation, so

$$(4.3) \quad u^n(x) = \rho^n e^{ikx} = \rho^n e^{i\xi x/\Delta x}, \quad \xi \in [-\pi, \pi],$$

where  $\rho^n = \rho^n(\xi)$  is the amplification factor associated with  $\xi$ . Plugging such *ansatz* into the stage values, we get

$$u_j^{(\ell)} = \rho^n \exp(i\xi(x_j - v\Delta t c_\ell)/\Delta x) = \rho^n e^{ij\xi} e^{-ic_\ell a\xi},$$

where  $a = v\Delta t/\Delta x$  denotes the CFL number. In [26], the relation between  $u(x)$  and  $\hat{u}$  is given by

$$\frac{\hat{u}(x + \Delta x/2) - \hat{u}(x - \Delta x/2)}{\Delta x} = \frac{\partial u}{\partial x}(x).$$

Using this relation and (4.3) one has

$$(4.4) \quad \hat{u}^n(x) = \frac{u^n(x)}{\text{sinc}(\xi/2)},$$

where  $\text{sinc}(x) = \sin(x)/x$ .

Making use (4.4) and (4.3) in Eq.(4.2), one obtains the following formula for the amplification factor:

$$(4.5) \quad \rho(\xi) = 1 - i\xi a \sum_{\ell=1}^s b_\ell \exp(-ic_\ell a\xi).$$

The scheme is stable if  $|\rho(\xi)| \leq 1$  for all  $\xi \in [-\pi, \pi]$ .

Such stability problem is closely related to the linear stability of the quadrature formula when applying to the approximation of the integral form of a scalar linear ODE,

$$y' = \lambda y, \quad y(0) = 1, \quad \forall \lambda \in \mathbb{C}.$$

In fact, the solution after one step of this ODE is:  $y(\Delta t) = e^{\lambda \Delta t} = e^z$ , where  $z := \Delta t \lambda$ . Such solution is stable iff  $\mathcal{R}(z) \leq 0$ , i.e. if  $\mathcal{R}(\lambda) \leq 0$ . Considering the following identity

$$e^z = 1 + z \int_0^1 e^{cz} dc$$

and approximating the integral by a quadrature formula with nodes  $c_\ell$  and weights  $b_\ell$ , one obtains the approximation of the exact solution after one step:

$$(4.6) \quad R(z) = 1 + z \sum_{\ell=1}^s b_\ell e^{c_\ell z}$$

with which the stability region can be drawn by the set  $\{z \in \mathbb{C} : |R(z)| \leq 1\}$ . Comparing equations (4.5) with (4.6), ones has  $\rho(\xi) = R(-ia\xi)$  with  $\xi \in [\pi, \pi]$ . Thus the stability of a quadrature formula in a conservative semi-Lagrangian scheme for a linear advection equation is closely related to the stability on the imaginary axis. Then in order to guarantee stability we look of the largest interval  $I^* = [-y^*, y^*]$  of the imaginary axis such that  $|R(iy)| \leq 1 \forall y \in I^*$ . Note that the bound  $a^* = y^*/\pi$  quantifies the maximum CFL number for the semi-Lagrangian scheme that guarantees stability.

Now in order to maximize the stability interval on imaginary axis, we construct quadrature formulas that allow a wider stability region. Let us consider the expression  $R(iy)$  and write it in the form

$$(4.7) \quad R(iy) = 1 + iy(C_s(y) + iS_s(y)) = 1 - yS_s(y) + iyC_s(y)$$

where

$$C_s(y) = \sum_{\ell=1}^s b_\ell \cos(c_\ell y), \quad S_s(y) = \sum_{\ell=1}^s b_\ell \sin(c_\ell y).$$

The stability condition therefore becomes

$$|R(iy)|^2 = 1 - 2yS_y(y) + y^2(C_s^2(y) + S_s^2(y)) \leq 1.$$

Such condition can be written in the form

$$(4.8) \quad yF_s(y) \geq 0, \text{ where } F_s(y) := S_y(y) - \frac{1}{2}(C_s^2(y) + S_s^2(y)).$$

Then the problem to find quadrature formulas with the widest stability region is connected to determine the coefficients  $\mathbf{b} = (b_1, \dots, b_s)$  and  $\mathbf{c} = (c_1, \dots, c_s)$  so that the interval in which (4.8) is satisfied is the widest. The analysis of quadrature formulas with even  $s$  and symmetric distribution of nodes around the middle of the interval is performed in [21].

Here we numerically compute nodes and weights for a particular class of third order DIRK schemes that satisfy the simplification conditions

$$\sum_{j=1}^s a_{ij} = c_i, \quad i = 1, \dots, s$$

and for which the last row of the  $A$ -matrix coincides with the weights,  $a_{s,j} = b_j$ ,  $j = 1, \dots, s$ . This constraint is imposed in order to have  $L$ -stable schemes, in view of the AP property in the fluid dynamic regime. Such schemes have the following structure:

$$(4.9) \quad \begin{array}{c|ccc} c_1 & c_1 & 0 & 0 \\ c_2 & c_2 - \gamma_2 & \gamma_2 & 0 \\ \hline 1 & b_1 & b_2 & b_3 \\ \hline & b_1 & b_2 & b_3 \end{array}$$

The coefficients of the scheme are determined taking into account the following requirements:

- the scheme has to be at least third order accurate;
- the scheme has to be  $A$ -stable (and therefore  $L$ -stable, because it is Stiffly Accurate, (SA) i.e.  $a_{si} = b_i$  for  $i = 1, 2, 3$ , see [13]);
- nodes and weight are selected in such a way that condition (4.8) is satisfied for a wide region.

Order conditions for scheme (4.9), up to third order accuracy, are:

$$(4.10) \quad \sum_{i=1}^s b_i = 1, \quad \sum_{i=1}^s b_i c_i = 1/2, \quad \sum_{i=1}^s b_i c_i^2 = 1/3, \quad \sum_{i,j=1}^s b_i a_{ij} c_j = 1/6.$$

Solving these equations allows to express four parameters of the scheme as a function of  $c_1$  and  $c_2$ :

$$(4.11) \quad b_2 = \frac{1}{6} \frac{3c_1 - 1}{(c_2 - c_1)(c_2 - 1)}, \quad b_3 = \frac{1}{6} \frac{6c_1 c_2 - 3c_1 - 3c_2 + 2}{(c_2 - 1)(c_1 - 1)}, \quad \gamma_2 = \frac{1}{2} \frac{6c_1^2 c_2 - 4c_1 c_2 - c_1 + c_2}{(3c_1 - 1)(c_1 - 1)}$$

and  $b_1 = 1 - b_2 - b_3$ . This leaves two free parameters, which are chosen according to the two additional conditions.

In order to impose  $A$ -stability, from [13], we recall the following result.

An implicit R-K method is  $A$ -stable iff

- (1) the stability function  $R(z) = P(z)/Q(z)$  is analytic in  $\mathbb{C}$  for  $\text{Re}(z) < 0$ ;
- (2) the method is  $I$ -stable, i.e.  $|R(iy)| \leq 1$  for all  $y \in \mathbb{R}$  (stability on the imaginary axis).

The  $I$ -stability is equivalent to the fact that the polynomial

$$(4.12) \quad E(y) = |Q(iy)|^2 - |P(iy)|^2 = \sum_{j=0}^s E_{2j} y^{2j}$$

satisfies  $E(y) \geq 0$  for all  $y \in \mathbb{R}$  and  $i = \sqrt{-1}$ .

Performing a detailed calculation (reported in Appendix C), the condition for  $I$ -stability (4.12) and (4.8) becomes: either

$$(4.13) \quad c_1 < 1/3, \quad c_2 > 1$$

or

$$(4.14) \quad c_1 > 1/3, \quad c_2 < 1.$$

The latter has to be excluded since it implies  $b_3 < 0$  and condition (1) for the analyticity of the function  $R(z)$  above is not satisfied.

Then DIRK scheme (4.9) is  $A$ -stable and by the SA property, it's also  $L$ -stable.

**Remark** If we look for a third order Singly DIRK scheme i.e. with  $\gamma_1 = \gamma_2 = \gamma_3 = \gamma$ , as in [3], then there are no free parameters, and one obtains  $\gamma \simeq 0.4358665215$  and  $\delta = \frac{3}{2}\gamma^2 - 5\gamma + \frac{5}{4} \simeq 644363171$ . This scheme is  $A$ -stable and  $L$ -stable, but the weights and the nodes do not satisfy condition (4.8) for any  $y > 0$ , i.e. scheme (4.2) is not stable.

This remark suggests to look for DIRK methods as (4.9) such that  $\gamma_1 = \gamma_3 = \gamma$ , i.e.

$$(4.15) \quad \begin{array}{c|ccc} \gamma & \gamma & 0 & 0 \\ \hline c_2 & c_2 - \gamma & \gamma & 0 \\ 1 & 1 - b_2 - \gamma & b_2 & \gamma \\ \hline & 1 - b_2 - \gamma & b_2 & \gamma \end{array}$$

From (4.10), we have four equations with five unknowns  $b_2$ ,  $c_2$ ,  $\gamma_2$ ,  $\gamma$  and  $b_1$  and from (4.11), with  $c_1 = b_3 = \gamma$ , we compute  $b_2$ ,  $c_2$  and  $\gamma_2$  as functions of  $\gamma$  and  $b_1 = 1 - b_2 - \gamma$ .

Performing a detailed calculation (reported in Appendix C), we require to choose  $\gamma$  in the following intervals

$$(4.16) \quad [1 - \sqrt{2}/2, 1/3[ \cup ]1 + \sqrt{2}/2, +\infty[.$$

Note that the second interval can not be accepted because this implies values of  $\gamma$  such that  $\gamma > 1 + \sqrt{2}/2 \approx 1.70710\dots$ , and this is in contradiction with the hypothesis (4.13).

A numerical experiment shows that the optimal value of  $\gamma$  in the first interval in order to have stability, is approximately  $\gamma = 0.3$ , (see Fig. 5). Then for this choice of  $\gamma$ , the coefficients of scheme (4.15) are:  $\gamma = 0.3$ ,  $\gamma_2 = 13/3$ ,  $b_2 = -3/710$  and  $c_2 = 8/3$ . This scheme is stable under the condition (4.8) for  $y \leq y^* = 4.715426442$  with  $a^* \approx 1.5$  and is also  $L$ -stable.

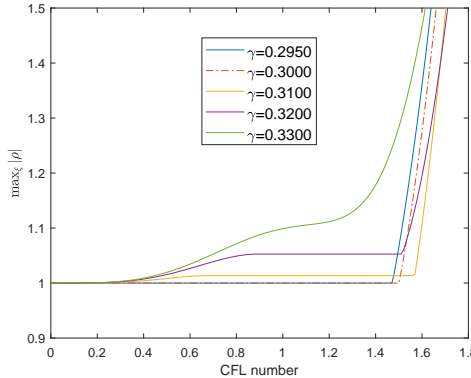


FIGURE 5. Optimal choice of  $\gamma$  for scheme (4.15).

For the numerical experiments, we use the following two types of DIRK methods. The first is a second order DIRK scheme (DIRK2) [3]

$$\text{DIRK2} = \begin{array}{c|cc} \alpha & \alpha & 0 \\ \hline 1 & 1-\alpha & \alpha \\ \hline & 1-\alpha & \alpha \end{array}$$

where  $\alpha = 1 - \frac{\sqrt{2}}{2}$ . This scheme is stable under the condition (4.8) for  $y \leq y^* = 4.586275880$  with  $a^* \approx 1.46$  and is also  $L$ -stable. The second one is the third order DIRK scheme (DIRK3) (4.15).

Now apply BDF schemes to system (4.1) with  $f = vu$ , and we get

$$(4.17) \quad u_j^{n+1} = \sum_{\ell=1}^k a_\ell u_j^{n-\ell+1} - \beta_k v \frac{\Delta t}{\Delta x} \left( \hat{u}_{j+1/2}^{n+1} - \hat{u}_{j-1/2}^{n+1} \right),$$

and by (4.4)

$$(4.18) \quad \hat{u}_{j+1/2}^{n+1} = \frac{\tilde{u}^{n+1}(x_{j+1/2})}{\text{sinc}(\xi/2)},$$

with

$$(4.19) \quad \tilde{u}^{n+1}(x_j) = \sum_{\ell=1}^k a_\ell u^n(x_j - v\ell\Delta t).$$

Then we look for the evolution of the Fourier mode identified by the parameter  $\xi \in [-\pi, \pi]$ . We set  $u(x) = \rho^n e^{ikx} = \rho^n e^{i\xi x/\Delta x}$  so that  $u^n(x_j) = u_j^n = \rho^n e^{ij\xi}$ . Then (4.19) becomes

$$\tilde{u}^{n+1}(x_j) = \sum_{\ell=1}^k a_\ell \rho^{n-\ell+1} e^{i\xi(x_j - \ell v\Delta t)/\Delta x},$$

and (4.18) becomes

$$\hat{u}^{n+1}(x_{j+1/2}) = \left( \sum_{\ell=1}^k a_\ell \rho^{n-\ell+1} e^{ij\xi} e^{-i\xi a} e^{i\xi/2} \right) / \text{sinc}(\xi/2),$$

After some algebraic manipulation, we obtain for (4.17):

$$(4.20) \quad \rho^{n+1} = \sum_{\ell=1}^k a_\ell \rho^{n-\ell+1} (1 - \beta_k a e^{-i\xi \ell a} i\xi)$$

where  $a = v\Delta t/\Delta x$ . Then the characteristic polynomial associated to (4.20) is:

$$(4.21) \quad p(\rho) = \rho^k - \sum_{\ell=1}^k a_\ell \rho^{k-\ell} (1 - \beta_k a e^{-i\xi \ell a} i\xi).$$

Now again we compute the maximum  $a^*$  such that

$$(4.22) \quad \max_{\xi \in [-\pi, \pi]} |\rho(a, \xi)| \leq 1, \quad \forall a \in [0, a^*].$$

Here  $\rho(a, \xi)$  represents the largest root in absolute value of the polynomial  $p(\rho)$ . In particular, we consider the two BDF schemes BDF2 and BDF3 with  $k = 2$  and  $k = 3$ , respectively. We compute numerically (4.22) and we get for BDF2  $a^* \approx 0.5678$ , while BDF3 is unstable for each  $a > 0$ .

This analysis confirms that the conservative correction imposes stability restriction on the CFL number  $a^*$  for the BDF methods.

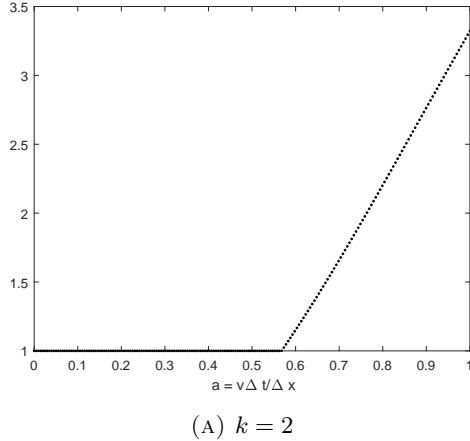
We conclude that C-SL schemes based on RK framework have better stability properties than those based on BDF when applied to linear advection equation (4.1).

Note that in our numerical tests in practise some schemes can be more stable when applied to BGK equation because the collision term has a stabilizing effect.

## 5. NUMERICAL EXPERIMENTS

In this section, we propose four tests to verify some properties of proposed schemes.

In test 1, we compute the conservation error of the schemes. In test 2, we check the correct order of accuracy for smooth solutions for various values of the Knudsen number  $\kappa$ . In test 2, we check the Asymptotic Preserving(AP) property. We end this section with test 3, in which we check shock capturing capability for the Euler limit. We only consider one-dimensional problems. For the time step, we use  $\Delta t = \text{CFL} \times \Delta x / |v_{\max}|$ . For space and velocity grids, we discretize  $\Delta v :=$

FIGURE 6. Optimal  $a^*$  for BDF2

$(v_{max} - v_{min})/N_v$  and  $\Delta x := (x_{max} - x_{min})/N_x$ . To distinguish proposed conservative schemes from non-conservative schemes, we denote each scheme as follows:

Scheme name	Conservative	ODE solver	Reconstruction	Maxwellian
RK2-W23-DM	YES	DIRK2	WENO 2-3	Discrete
RK3-W35-DM	YES	DIRK3	WENO 3-5	Discrete
RK2-W23	NO	DIRK2	WENO 2-3	Continuous
RK3-W35	NO	DIRK3	WENO 3-5	Continuous

A similar notation is used for the schemes based on BDF time integrator.

**5.1. Test 1.** We consider the same single shock test adopted in Section 2.2, and apply the various schemes based on the conservative correction. The results are summarized in Tables 4 and 5.

$(N_x, N_v)$	RK3-W35-CM			RK3-W35-DM		
	Mass	Momentum	Energy	Mass	Momentum	Energy
(100, 40)	3.74e-07	1.51e-05	4.07e-06	5.47e-15	7.52e-14	8.59e-14
(100, 50)	5.80e-12	3.58e-10	9.66e-11	5.55e-14	4.04e-13	5.22e-13
(100, 60)	1.70e-13	1.45e-13	3.25e-13	1.92e-13	1.45e-13	3.43e-13
(100, 90)	1.47e-13	8.85e-14	1.85e-13	1.30e-13	8.51e-14	2.27e-13
(200, 40)	7.70e-07	4.37e-06	8.38e-06	1.28e-14	2.39e-15	7.45e-14
(200, 50)	1.21e-11	1.03e-10	1.99e-10	2.13e-13	3.04e-13	2.59e-13
(200, 60)	3.63e-13	1.74e-14	1.28e-13	3.73e-13	8.07e-14	1.79e-13
(200, 90)	2.85e-13	1.47e-13	1.51e-13	2.83e-13	1.62e-13	1.75e-13

TABLE 4. RK-based schemes,  $CFL = 2$ . Conservation error of discrete moments in relative  $L_1$  norm for Test 1. Comparison between continuous one (CM) and discrete Maxwellian (DM)

When using with the continuous Maxwellian with the conservative correction, a negligible conservation error can be achieved, but only using a large enough number of velocity grid points. In contrast, conservation error can be suppressed to a negligible level with relatively small number of velocity grid points when the discrete Maxwellian is used (See Table 4 and 5 with  $N_v = 40$ ). We present the conservation error estimates in Appendix D.

It appears that the combined use of discrete Maxwellian and conservative correction provides a scheme which maintains conservation within round-off error. In particular, the use of discrete

$(N_x, N_v)$	BDF3-W35-CM			BDF3-W35-DM		
	Mass	Momentum	Energy	Mass	Momentum	Energy
(100, 40)	2.13e-07	6.30e-07	2.31e-06	3.55e-15	6.50e-15	3.40e-15
(100, 50)	3.33e-12	1.50e-11	5.47e-11	6.08e-14	6.09e-14	3.43e-14
(100, 60)	1.05e-13	1.95e-14	1.61e-14	1.06e-13	3.42e-15	6.49e-15
(100, 90)	8.12e-14	1.16e-14	1.17e-14	8.39e-14	3.25e-14	1.54e-14
(200, 40)	4.31e-07	2.19e-06	4.68e-06	1.49e-14	3.08e-14	3.80e-14
(200, 50)	6.78e-12	5.22e-11	1.11e-10	1.60e-13	8.65e-14	1.51e-14
(200, 60)	1.80e-13	4.75e-14	3.68e-14	1.82e-13	5.61e-14	4.48e-14
(200, 90)	1.34e-13	8.03e-14	3.77e-14	1.36e-13	8.99e-14	4.42e-14

TABLE 5. BDF-based schemes,  $CFL = 2$ . Conservation error of discrete moments in relative  $L_1$  norm for Test 1. Comparison between continuous one (CM) and discrete Maxwellian (DM)

Maxwellian allows to maintain conservation with a small number of velocity nodes, which is particularly useful when adopting the method to capture the fluid dynamic limit for small Knudsen number.

**5.2. Test 2.** This test is proposed in [12] to check the accuracy of the scheme. The initial condition for the distribution function is the Maxwellian

$$f_0(x, v) = \frac{\rho_0}{\sqrt{2\pi T_0}} \exp\left(-\frac{|v - u_0(x)|^2}{2T_0}\right),$$

where initial velocity profile is given by

$$u_0(x) = 0.1 \exp(-(10x - 1)^2) - 2 \exp(-(10x + 3)^2).$$

Initial density and temperature are uniform, with constant value  $\rho_0(x) = 1$  and  $T_0(x) = 1$ . We use the periodic boudndary condition. The computation is performed on  $(x, v) \in [-1, 1] \times [-10, 10]$ . Since shock appears for  $\kappa = 10^{-6}$  at  $t = 0.35$ , the final time is taken  $T_f = 0.32$ . We take  $N_x = 160, 320, 640, 1280, 2560$ , and 5120 and uniform grid points in  $x$  direction and  $N_v = 20$  uniform grid points in  $v$  direction. We have used differnt CFL based on the stability analysis. For RK schemes, we choose  $CFL = 2$ . For BDF2 and BDF3, we set  $CFL = 0.5$ . We compute the relative  $L^1$  norm to check the accuracy.

**5.3. Test 3.** To check the AP property of the C-SL scheme, we take a similar test as in [27]. We check numerically  $\|f - M\|_1 = \mathcal{O}(\kappa)$  for different values of  $\kappa = 10^{-4}, 10^{-5}, 10^{-6}, 10^{-7}$ .

We take the following non-equilibrium initial data

$$f_0(x, v) = 0.5 \left( \frac{\rho_0(x)}{\sqrt{2\pi T_0(x)}} \exp\left(-\frac{(v - u_0(x))^2}{2T_0(x)}\right) + \frac{\rho_0(x)}{\sqrt{2\pi T_0(x)}} \exp\left(-\frac{(v + u_0(x))^2}{2T_0(x)}\right) \right),$$

where initial density, velocity and temperature are given by

$$\rho_0(x) = \frac{2 + \sin 2\pi x}{3}, \quad u_0(x) = \frac{\cos 2\pi x}{5}, \quad T_0(x) = \frac{3 + \cos 2\pi x}{4}.$$

We use the periodic boundary condition. The computation is performed on  $x \in [-1, 1]$ ,  $v \in [-8, 8]$ . The final time is taken 0.02.

We implemented RK3-W35-DM and BDF3-W35-DM with  $N_x = 100$  and  $CFL = 1$ . In Figures 7–10, we show the time evolution of  $\|f - M\|_1$  for our C-SL scheme for different values of  $\kappa$  and different values for the number of grid points in velocity space, i.e.,  $N_v = 20, 32$ .

From the figures it appears that the norm of the difference between  $f$  and the Maxwellian is roughly proportional to the Knudsen number  $\kappa$ , es expected. If a continuous Maxwellian, such a norm depends also on the number of velocity grid points, as appears in see Fig. 7 (A) and in Fig. 9 (A), where with  $N_v = 20$  the difference does not decrease significantly when going from  $\kappa = 10^{-7}$  to  $\kappa = 10^{-8}$ . On

Test 2 RK2-W23-DM Mass, CFL=2								
	$\kappa = 10^{-6}$		$\kappa = 10^{-4}$		$\kappa = 10^{-2}$		$\kappa = 10^{-0}$	
$N_x$	error	rate	error	rate	error	rate	error	rate
160-320	1.01e-03	1.74	9.80e-04	1.79	1.79e-04	2.17	7.13e-04	1.69
320-640	3.02e-04	1.78	2.84e-04	1.86	3.97e-05	2.06	2.21e-04	1.84
640-1280	8.83e-05	2.17	7.82e-05	2.29	9.54e-06	2.01	6.19e-05	2.12
1280-2560	1.96e-05	2.38	1.60e-05	2.37	2.37e-06	1.99	1.42e-05	2.53
2560-5120	3.76e-06		3.09e-06		5.95e-07		2.47e-06	
Test 2 BDF2-W23-DM Mass, CFL=0.5								
	$\kappa = 10^{-6}$		$\kappa = 10^{-4}$		$\kappa = 10^{-2}$		$\kappa = 10^{-0}$	
$N_x$	error	rate	error	rate	error	rate	error	rate
160-320	1.01e-03	1.74	9.80e-04	1.78	1.77e-04	2.17	7.09e-04	1.68
320-640	3.03e-04	1.77	2.85e-04	1.86	3.93e-05	2.05	2.21e-04	1.84
640-1280	8.86e-05	2.18	7.84e-05	2.29	9.46e-06	2.01	6.19e-05	2.13
1280-2560	1.96e-05	2.38	1.60e-05	2.37	2.35e-06	1.99	1.42e-05	2.53
2560-5120	3.75e-06		3.09e-06		5.93e-07		2.45e-06	
Test 2 RK3-W35-DM Mass, CFL=2								
	$\kappa = 10^{-6}$		$\kappa = 10^{-4}$		$\kappa = 10^{-2}$		$\kappa = 10^{-0}$	
$N_x$	error	rate	error	rate	error	rate	error	rate
160-320	5.74e-05	3.31	5.07e-05	3.47	2.28e-06	4.34	1.28e-05	4.74
320-640	5.77e-06	4.23	4.58e-06	4.39	1.12e-07	3.59	4.80e-07	4.88
640-1280	3.08e-07	4.61	2.19e-07	4.43	9.31e-09	3.09	1.63e-08	4.66
1280-2560	1.26e-08	4.28	1.02e-08	3.58	1.09e-09	2.98	6.43e-10	4.06
2560-5120	6.49e-10		8.50e-10		1.38e-10		3.84e-11	
Test 2 BDF3-W35-DM Mass, CFL=0.5								
	$\kappa = 10^{-6}$		$\kappa = 10^{-4}$		$\kappa = 10^{-2}$		$\kappa = 10^{-0}$	
$N_x$	error	rate	error	rate	error	rate	error	rate
160-320	5.59e-05	3.30	4.93e-05	3.47	1.93e-06	4.99	1.26e-05	4.81
320-640	5.69e-06	4.28	4.44e-06	4.47	6.07e-08	5.31	4.47e-07	5.18
640-1280	2.93e-07	4.77	2.01e-07	4.90	1.53e-09	4.61	1.24e-08	5.00
1280-2560	1.07e-08	4.96	6.72e-09	4.98	6.27e-11	2.38	3.85e-10	2.95
2560-5120	3.45e-10		2.13e-10		1.20e-11		5.00e-11	

TABLE 6. Test 2: convergence rate for second and third order RK and BDF schemes. A final time  $T_f = 0.32$  is selected such that the solution is still smooth even in the limit of vanishing Knudsen number. For such small time, space error appears to be dominant, and this explains the order of accuracy higher than expected from the order of the RK or BDF schemes. Some order reduction is observed in intermediate regimes.

the contrary, when using a discrete Maxwellian, the discrepancy between  $f$  and the Maxwellian only depends on the Knudsen number:  $\|f - \mathcal{M}\|_1 = \mathcal{O}(\kappa)$ .

The proposed C-SL scheme (3.1) is an asymptotic preserving (AP) scheme for the kinetic equation (1.1), that is, it becomes a consistent scheme for the underlying hydrodynamic limit. Note that in a recent review on AP schemes for kinetic and hyperbolic equations [16], a necessary condition to be AP for a scheme for BGK model (1.1) is that the solution  $f^n$  must be driven to the local equilibrium  $\mathcal{M}^n$  when  $\kappa \rightarrow 0$

$$(5.1) \quad f^n - \mathcal{M}(f^n) = \mathcal{O}(\kappa), \quad \text{for } n \geq 1$$

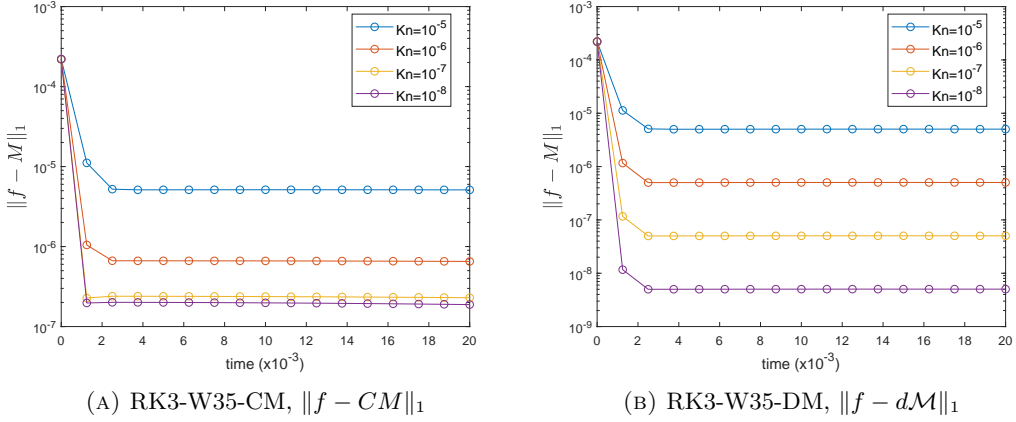


FIGURE 7. Time evolution of  $\|f - M\|_1$  for high order methods for the BGK model.  $N_v = 20$ . When using the continuous Maxwellian (left panel), the discrepancy between the distribution function and the Maxwellian saturates for small values of the Knudsen number, while the method based on the discrete Maxwellian (right panel) shows the expected behaviour  $\|f - M\|_1 = \mathcal{O}(\kappa)$ .

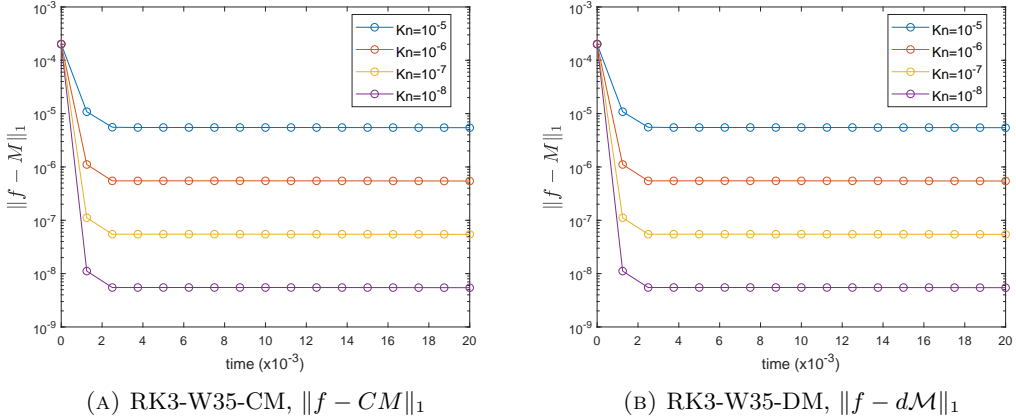


FIGURE 8. Time evolution of  $\|f - M\|_1$  for high order methods for the BGK model.  $N_v = 32$ . For large enough number of velocity grid points the discrepancy between the function and the Maxwellian appears to be proportional to  $\kappa$ , up to  $\kappa = 10^{-8}$ , for both schemes.

for any initial data  $f^0$ , namely, the numerical solution projects any data into the local equilibrium  $\mathcal{M}^n$ , with an accuracy of  $\mathcal{O}(\kappa)$ , in one step. Such AP schemes are referred to as *strongly* AP.

**5.4. Test 4.** The final test is the classical Riemann problem. To observe the Euler limit, we take  $\kappa = 10^{-6}$ . Moreover, to see the influence of the conservative correction, we compare our scheme with the standard non-conservative semi-Lagrangian scheme. Initial condition is given by the Maxwellian computed from

$$(\rho_0, u_0, p_0) = \begin{cases} (2.25, 0, 1.125), & \text{for } x \leq 0.5 \\ (3/7, 0, 1/6), & \text{for } x > 0.5 \end{cases}$$

We use freeflow boundary condition. Computations are performed on  $x \in [0, 1]$ ,  $v \in [-10, 10]$  upto final time  $T_f = 0.16$ . With small Knudsen number, both conservative and non-conservative schemes are stable and they enable us to use  $\text{CFL} = 2$ . We take  $N_x = 200$  for both schemes. For

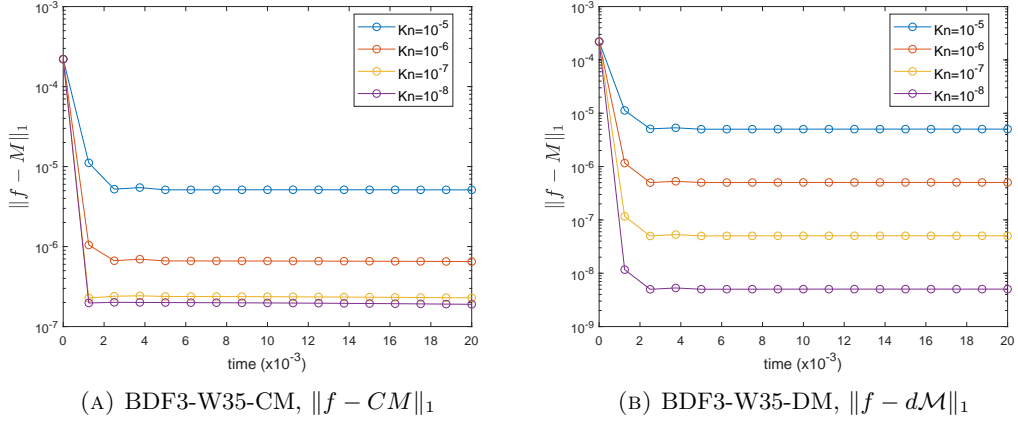


FIGURE 9. Same as Figure 7, but with BDF based schemes

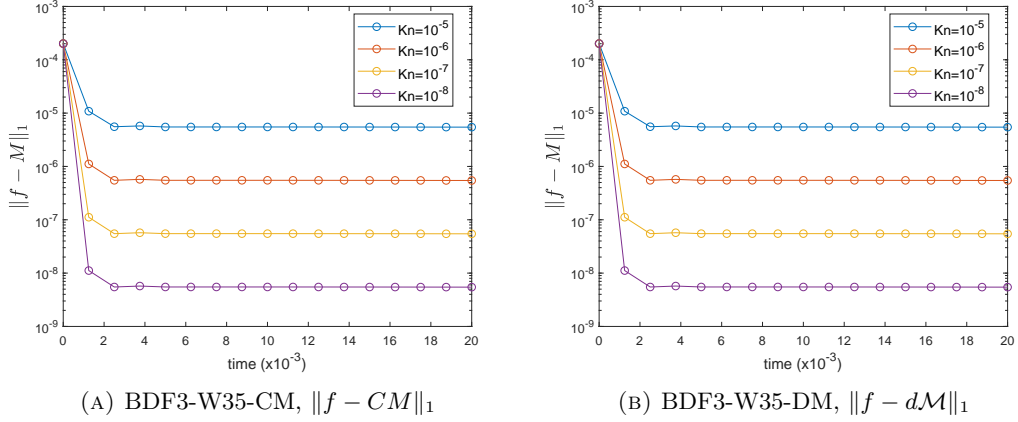


FIGURE 10. Same as Figure 8, but with BDF based schemes

the proposed schemes, RK3-W35-DM and BDF3-W35-DM, we take  $N_v = 30$ . For non-conservative schemes, RK3W35 and BDF3W35, we take  $N_v = 60$ . The larger number of velocity grid points ensures that the conservation error due to the use of continuous Maxwellian is negligible with respect to the one due to lack of conservation of the transport term. The results are shown in Figure 11. It appears that conservative schemes capture shocks correctly and are in perfect agreement with the exact reference solution.

## 6. CONCLUSIONS

In this paper we present high order conservative semi-lagrangian schemes for the numerical solution of the BGK model of the Boltzmann equation. Conservation properties are obtained by using a discrete Maxwellian in the collision operator, and by a conservative correction of the advection term. Exact conservation can be reached up to round-off errors. Together with L-stable treatment of the collisions, exact conservation allows the construction of schemes which become consistent *shock-capturing* schemes for the underlying Euler limit, as the Knudsen number  $\kappa$  vanishes (AP property), even when using a relatively small number of grid points in velocity.

The conservation properties, and the consequent AP property, have been proven mathematically and verified in several numerical tests. A drawback of the conservative correction procedure is the limitation it imposes on the stability of the schemes. A stability analysis has been performed to

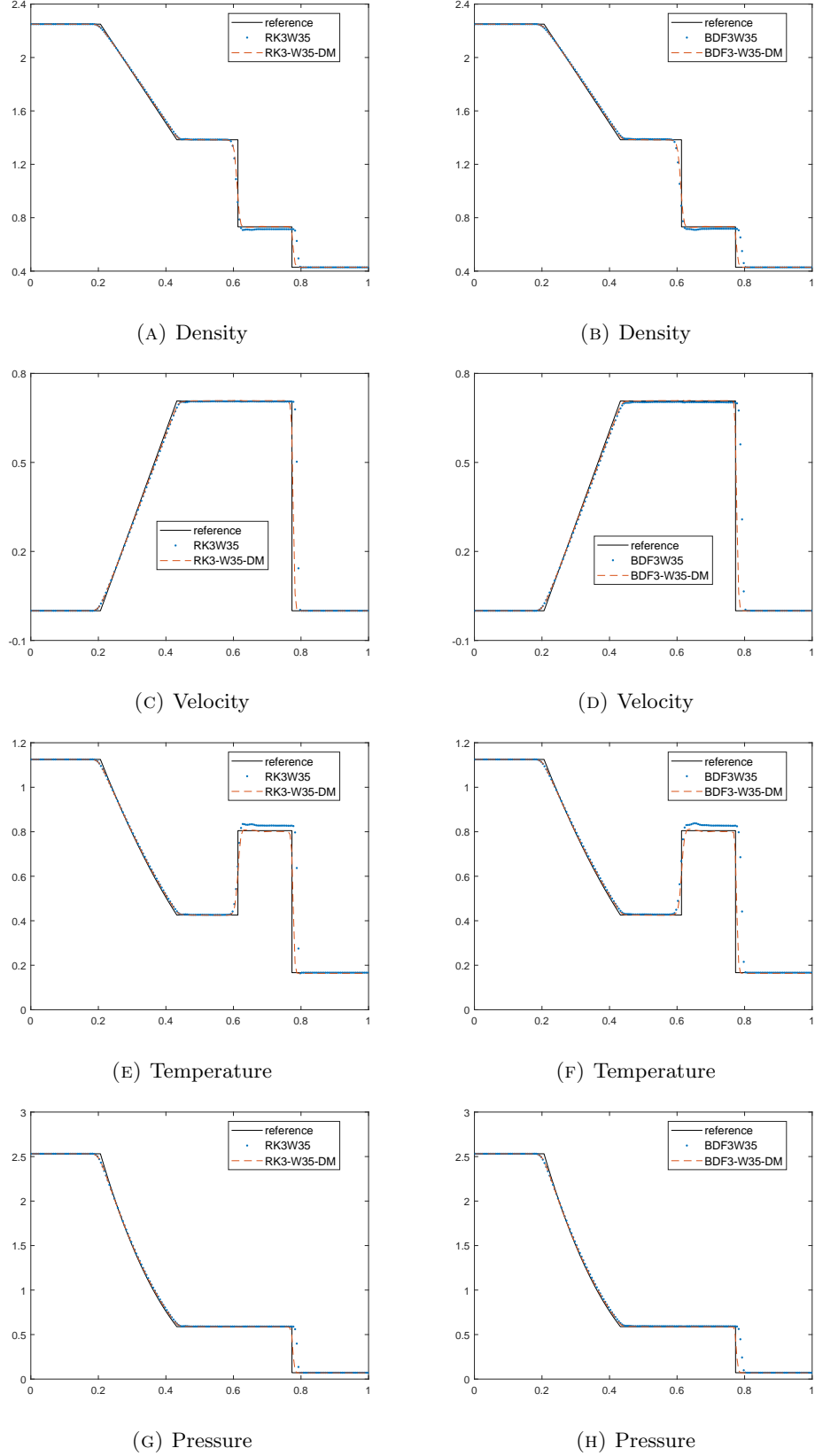


FIGURE 11. Riemann problem in 1D space and velocity with  $\kappa = 10^{-6}$ . From top to bottom: Density, Velocity, Temperature and Pressure. Red crosses: standard SL schemes, blue squares: new conservative schemes, black line: exact solution.

understand the reason of such limitation. It is observed that Runge-Kutta based schemes have a wider stability region than multistep-bases ones, with a net improvement over Eulerian based schemes for all Knudsen numbers. Stability restrictions become less severe for small Knudsen numbers, making the schemes competitive in such regimes.

In this paper, we only consider 1D case in both space and velocity. However, the technique is quite general and can be applied to the multi-dimensional case.

As a work in progress, we are developing new conservative semi-lagrangian schemes that do not suffer from such a CFL limitation, which will be the subject of a forthcoming paper.

#### APPENDIX A. PROOF OF THE ESTIMATE ON THE CONSERVATION ERROR FOR IE-SL SCHEME WITH THE DISCRETE MAXWELLIAN

Let us check in what sense the scheme (2.8) has a better conservative nature compared to that of (2.4). For this, we first rewrite (2.8) as

$$(A.1) \quad f_{i,j}^{n+1} - \tilde{f}_{ij}^n = \frac{\Delta t}{\kappa + \Delta t} \left( d\mathcal{M}(\tilde{f}_{ij}^n) - \tilde{f}_{ij}^n \right),$$

where  $\tilde{f}_{ij}^n = \theta_j f_{i^*+1,j}^n + (1 - \theta_j) f_{i^*,j}^n$  with  $i^* = \lfloor i - v_j \Delta t / \Delta x \rfloor$ ,  $\theta_j = (x_i - \tilde{x}_j) / \Delta x$ .

Since  $\theta_j$  does not depend on  $i$ , we find that the following telescoping cancellation holds so that  $f_{i,j}^n$  and  $\tilde{f}_{ij}^n$  share the first moment:

$$(A.2) \quad \sum_{i=1}^{N_x} \tilde{f}_{ij}^n = \sum_{i=1}^{N_x} (\theta_j f_{i^*+1,j}^n + (1 - \theta_j) f_{i^*,j}^n) = \sum_{i=1}^{N_x} f_{i,j}^n.$$

Multiplying (A.1) by  $\phi(v_j) = (1; v_j; v_j^2/2)$ , taking summation on  $i, j$  and inserting (A.2), one gets

$$\sum_{i=1}^{N_x} \sum_{j=0}^{N_v} (f_{i,j}^{n+1} - f_{i,j}^n) \phi(v_j) \Delta v \Delta x = \frac{\Delta t}{\kappa + \Delta t} \sum_{i=1}^{N_x} \sum_{j=0}^{N_v} \left( d\mathcal{M}(\tilde{f}_{ij}^n) - \tilde{f}_{ij}^n \right) \phi(v_j) \Delta v \Delta x.$$

Summing further in time step, we have

$$(A.3) \quad \begin{aligned} & \sum_{i=1}^{N_x} \sum_{j=0}^{N_v} (f_{i,j}^{N_t} - f_{i,j}^0) \phi(v_j) \Delta v \Delta x \\ &= \frac{\Delta t}{\kappa + \Delta t} \sum_{k=0}^{N_t-1} \sum_{i=1}^{N_x} \sum_{j=0}^{N_v} \left( d\mathcal{M}(\tilde{f}_{ij}^k) - \tilde{f}_{ij}^k \right) \phi(v_j) \Delta v \Delta x, \end{aligned}$$

then, denoting the  $\ell$ th component of  $\phi(v_j)$  by  $\phi_\ell(v_j)$ ,  $\ell = 1, 2, 3$ , and using a variant of (2.7):

$$(A.4) \quad \max_{1 \leq \ell \leq 3} \left| \sum_{j=0}^{N_v} \left[ d\mathcal{M}(\tilde{f}_{ij}^k) - \tilde{f}_{ij}^k \right] \phi_\ell(v_j) \Delta v \right| < tol,$$

we obtain the following estimate:

$$\begin{aligned} & \max_{1 \leq \ell \leq 3} \left| \sum_{i=1}^{N_x} \sum_{j=0}^{N_v} (f_{i,j}^{N_t} - f_{i,j}^0) \phi_\ell(v_j) \Delta v \Delta x \right| \\ & \leq \frac{\Delta t}{\kappa + \Delta t} \sum_{k=0}^{N_t-1} \sum_{i=1}^{N_x} \max_{1 \leq \ell \leq 3} \left| \sum_{j=0}^{N_v} \left( d\mathcal{M}(\tilde{f}_{ij}^k) - \tilde{f}_{ij}^k \right) \phi_\ell(v_j) \Delta v \right| \Delta x \\ & \leq \frac{N_t \Delta t}{\kappa + \Delta t} (x_{max} - x_{min}) tol. \end{aligned}$$

This estimate tells us that error is stacked in each time step by  $tol$ . So, the total conservation error in the end essentially depends on  $N_t \times tol$  uniformly in  $\kappa$ . Therefore,  $tol$  should be taken small enough to attain a machine precision conservation error.

## APPENDIX B. GENERAL FRAMEWORK OF G-WENO INTERPOLATION

In this section, we illustrate the G-WENO interpolation of degree  $2n - 1$ . Let  $U = \{u_j\}, j \in I$  be a set of given values of a function  $u$  on a space grid  $x_j, j \in I$ .

We start with the Lagrange polynomial  $Q(x)$  built on the stencil  $S = \{x_{j-n+1}, \dots, x_{j+n}\}$ :

$$(B.1) \quad Q(x) = \sum_{k=1}^n C_k(x) P_k(x),$$

where the “linear weights”  $C_k(x)$  are polynomials of degree  $n - 1$  and  $P_k$  are polynomials of degree  $n$  interpolating  $U$  on the stencil  $S_k = \{x_{j-n+k}, \dots, x_{j+k}\}$ ,  $k = 1, \dots, n$ . The linear weights  $C_k(x)$  ( $k = 1, \dots, n$ ) are determined to satisfy the following two properties [7]:

- (1)  $C_k(x_i) = 0$  for  $x_i \in S - S_k$ .
- (2)  $\sum_k C_k(x_i) = 1$  for  $x_i \in S$ .

To guarantee non-oscillatory property, we replace the linear weights  $C_k(x)$  by the non-linear weights  $\omega_k(x)$ :

$$(B.2) \quad \omega_k(x) = \frac{\alpha_k(x)}{\sum_l \alpha^l(x)},$$

where  $\alpha_k(x)$  is defined by

$$(B.3) \quad \alpha_k(x) = \frac{C_k(x)}{(\beta_k + \epsilon)^2},$$

with the choice of  $\epsilon = 10^{-6}$ . The smoothness indicators  $\beta_k$  in (B.3) is defined by

$$(B.4) \quad \beta_k = \sum_{l=1}^n \int_{x_j}^{x_{j+1}} \Delta x^{2l-1} (P_k^{(l)})^2 dx.$$

The nonlinear weights  $\omega_k(x)$  are designed to put more weights on the smooth part of  $u$  and less weights on the discontinuous part of  $u$ .

Finally, the G-WENO reconstruction of the values  $U = \{u_j\}_{j \in I}$  reads

$$I[U](x) = \sum_{k=1}^n \omega_k(x) P_k(x)$$

In the following, we explicitly construct the G-WENO interpolations of order 3 and 5.

**B.1. G-WENO of order 3 (WENO23).** The G-WENO interpolation of order 3 can be represented with two second order polynomials  $P_L$  and  $P_R$  built respectively on stencils  $\{x_{j-1}, x_j, x_{j+1}\}$  and  $\{x_j, x_{j+1}, x_{j+2}\}$ :

$$P(x) = \omega_L P_L(x) + \omega_R P_R(x),$$

where the non-linear weights  $\omega_L$  and  $\omega_R$  are given by

$$(B.5) \quad \omega_\ell = \frac{\alpha_\ell}{\sum_\ell \alpha_\ell}, \quad \alpha_\ell = \frac{C_\ell}{(\epsilon + \beta_\ell)^2}, \quad \ell = L, R$$

with

$$C_L = \frac{x_{j+2} - x}{3\Delta x}, \quad C_R = \frac{x - x_{j-1}}{3\Delta x},$$

and

$$\begin{aligned}\beta_L &= \frac{13}{12}v_{j-1}^2 + \frac{16}{3}v_j^2 + \frac{25}{12}v_{j+1}^2 - \frac{13}{3}v_{j-1}v_j + \frac{13}{6}v_{j-1}v_{j+1} - \frac{19}{3}v_jv_{j+1} \\ \beta_R &= \frac{13}{12}v_j^2 + \frac{16}{3}v_{j+1}^2 + \frac{25}{12}v_{j+2}^2 - \frac{13}{3}v_jv_{j+1} + \frac{13}{6}v_jv_{j+2} - \frac{19}{3}v_{j+1}v_{j+2}.\end{aligned}$$

**B.2. G-WENO of order 5 (WENO35).** For the G-WENO interpolation of order 5, we use third order polynomials  $P_L$ ,  $P_C$  and  $P_R$  built respectively on stencils  $\{x_{j-2}, x_{j-1}, x_j, x_{j+1}\}$ ,  $\{x_{j-1}, x_j, x_{j+1}, x_{j+2}\}$  and  $\{x_j, x_{j+1}, x_{j+2}, x_{j+3}\}$ :

$$P(x) = \omega_L P_L(x) + \omega_C P_C(x) + \omega_R P_R(x),$$

where the non-linear weights  $\omega_L$ ,  $\omega_C$  and  $\omega_R$  are given by

$$\omega_\ell = \frac{\alpha_\ell}{\sum_\ell \alpha_\ell}, \quad \alpha_\ell = \frac{C_\ell}{(\epsilon + \beta_\ell)^2}, \quad \ell = L, C, R$$

with

$$C_L = \frac{(x - x_{j+2})(x - x_{j+3})}{20\Delta x^2}, \quad C_C = -\frac{(x - x_{j-2})(x - x_{j+3})}{10\Delta x^2}, \quad C_R = \frac{(x - x_{j-2})(x - x_{j-1})}{20\Delta x^2}$$

and

$$\begin{aligned}\beta_L &= \frac{407}{90}v_{j+1}^2 + \frac{721}{30}v_j^2 + \frac{248}{15}v_{j-1}^2 + \frac{61}{45}v_{j-2}^2 - \frac{1193}{60}v_{j+1}v_{j-2} + \frac{439}{30}v_{j+1}v_{j-1} \\ &\quad - \frac{683}{180}v_{j+1}v_{j-2} - \frac{2309}{60}v_jv_{j-1} + \frac{309}{30}v_jv_{j-2} - \frac{553}{60}v_{j-1}v_{j-2} \\ \beta_C &= \frac{61}{45}v_{j-1}^2 + \frac{331}{30}v_j^2 + \frac{331}{30}v_{j+1}^2 + \frac{61}{45}v_{j+2}^2 - \frac{141}{20}v_{j-1}v_j + \frac{179}{30}v_{j-1}v_{j+1} \\ &\quad - \frac{293}{180}v_{j-1}v_{j+2} - \frac{1259}{60}v_jv_{j+1} + \frac{179}{30}v_jv_{j+2} - \frac{141}{20}v_{j+1}v_{j+2} \\ \beta_R &= \frac{407}{90}v_j^2 + \frac{721}{30}v_{j+1}^2 + \frac{248}{15}v_{j+2}^2 + \frac{61}{45}v_{j+3}^2 - \frac{1193}{60}v_jv_{j+3} + \frac{439}{30}v_jv_{j+2} \\ &\quad - \frac{683}{180}v_jv_{j+3} - \frac{2309}{60}v_{j+1}v_{j+2} + \frac{309}{30}v_{j+1}v_{j+3} - \frac{553}{60}v_{j+2}v_{j+3}.\end{aligned}$$

### APPENDIX C. DETAILS ON THE STABILITY ANALYSIS

Here we find conditions such that Eq. (4.12) is satisfied. In order to make clear the calculation in the method (4.9) we take  $c_1 = \gamma_1$  and  $b_3 = \gamma_2$  then we get for the stability function (see [13]). Note that it is sufficient to have all  $E_{2j} \geq 0$  for the  $I$ -stability. These are the conditions that we actually use, in order to simplify the analysis.

We consider

$$(C.1) \quad R(z) = \frac{P(z)}{Q(z)} = \frac{p_0 + p_1z + p_2z^2 + p_3z^3}{q_0 - q_1z + q_2z^2 - q_3z^3}$$

with the following quantities:

$$(C.2) \quad p_0 = 1, \quad p_1 = \left(\frac{q_0}{1!} - \frac{q_1}{0!}\right), \quad p_2 = \left(\frac{q_0}{2!} - \frac{q_1}{1!} + \frac{q_2}{0!}\right), \quad p_3 = \left(\frac{q_0}{3!} - \frac{q_1}{2!} + \frac{q_2}{1!} - \frac{q_3}{0!}\right)$$

and

$$(C.3) \quad q_0 = 1, \quad q_1 = \gamma_1 + \gamma_2 + \gamma_3, \quad q_2 = \gamma_1\gamma_2 + \gamma_1\gamma_3 + \gamma_2\gamma_3, \quad q_3 = \gamma_1\gamma_2\gamma_3$$

and from (4.12) we have

$$(C.4) \quad E_2 = (q_1^2 - p_1^2) - 2(q_2q_0 - p_2p_0) \geq 0,$$

$$(C.5) \quad E_4 = (q_2^2 - p_2^2) - 2(q_3q_1 - p_3p_1) \geq 0,$$

$$(C.6) \quad E_6 = q_3^2 - p_3^2 \geq 0.$$

By (C.3) it follows  $E_2 = 0$ , and by SA we have  $R(\infty) = 0$ , and from (C.1) we get  $p_3 = 0$  and then  $E_6 = q_3^2 \geq 0$ . Now we compute  $E_4$ , and by (C.2-C.3) we get  $E_4 = (q_2^2 - p_2^2) - 2q_3q_1$ . From  $p_3 = 0$ , it follows

$$p_3 = \frac{1}{6} - \frac{q_1}{2} + q_2$$

and substituting we obtain  $E_4 = 8q_1 - 12q_2 - 3 \geq 0$ .

Now if we substitute the quantities (C.3) in  $E_4$ , and using (4.11) we get a function that depends on  $\gamma_1$  and  $c_2$

$$-\frac{S}{(3\gamma_1 - 1)(\gamma_1 - 1)^2(c_2 - 1)} \geq 0$$

with

$$S = (108c_2^2 - 72c_2 + 18)\gamma_1^4 + (-144c_2^2 + 105c_2 - 33)\gamma_1^3 + (84c_2^2 - 69c_2 + 24)\gamma_1^2 + (-24c_2^2 + 21c_2 - 7)\gamma_1 + 3c_2^2 - 3c_2 + 1.$$

The function  $S$  is always positive for  $\gamma_1 = c_2 \geq 0$ , then we have that  $E_4 \geq 0$ , if

$$\gamma_1 \leq 1/3, c_2 \geq 1, \text{ or } \gamma_1 \geq 1/3, c_2 \leq 1.$$

Now in order to justify the requirement to choose  $\gamma$  in the intervals (4.16) we consider again  $E_4 = 8q_1 - 12q_2 - 3 \geq 0$ .

In (4.15) with  $\gamma_1 = \gamma_3 = \gamma$ , we compute from (4.11)  $b_2$ ,  $c_2$  and  $\gamma_2$  as functions of  $\gamma$ :

$$(C.7) \quad b_2 = -\frac{3}{4} \frac{(2\gamma^2 - 4\gamma + 1)^2}{3\gamma^3 - 9\gamma^2 + 6\gamma - 1}, \quad c_2 = \frac{1}{3} \frac{(6\gamma^2 - 9\gamma + 2)}{(2\gamma^2 - 4\gamma + 1)}, \quad \gamma_2 = \frac{1}{3} \frac{(6\gamma^2 - 6\gamma + 1)}{(2\gamma^2 - 4\gamma + 1)}$$

and  $b_1 = 1 - b_2 - \gamma$ . Furthermore it follows:  $q_1 = (2\gamma + \gamma_2)$  and  $q_2 = (2\gamma_2\gamma + \gamma^2)$  and substituting this values in  $E_4$  we get

$$(C.8) \quad \gamma_2 \geq \frac{3 - 16\gamma + 12\gamma^2}{8 - 24\gamma}.$$

Now substituting  $\gamma_2$  from (C.7) in (C.8) and solving this inequality for  $\gamma$  we get (4.16).

#### APPENDIX D. CONSERVATION ERROR ESTIMATES FOR DISCRETE MOMENTS

In this section, we carry out some elementary conservation error estimate for each of the schemes derived so far. For simplicity we denote macroscopic moments  $m_i^n := (\rho_i^n, \rho_i^n U_i^n, E_i^n)^T$ , final time  $T^f$  and tolerance  $tol$ .

Now, we give discrete conservation error estimates with high order C-SL schemes with the discrete Maxwellian.

**Proposition D.1.** *In the periodic boundary condition, conservation error estimates for the DIRK scheme of order  $s = 1, 2, 3$  in mass, momentum and energy are given by*

$$\left\| \sum_{i=1}^{N_x} (m_i^{N_t} - m_i^0) \Delta x \right\|_{\infty} \leq \left( \sum_{k=1}^{s-1} |b_k| + |b_s| \right) \frac{N_t \Delta t}{\kappa + b_s \Delta t} (x_{max} - x_{min}) tol.$$

where  $b_k$ ,  $k = 1, \dots, s$  are determined for each  $s = 1, 2, 3$

*Proof.* The DIRK scheme of order  $s$  is given by

$$(D.1) \quad f_{i,j}^{n+1} = f_{i,j}^{*n+1} + \frac{\Delta t}{\kappa} \sum_{k=1}^s b_k \left( d\mathcal{M}_{i,j}^{(k),n+1} - f_{i,j}^{(k),n+1} \right),$$

where  $f_{i,j}^{*n+1} = f_{i,j}^n - \sum_{k=1}^s b_k \frac{\Delta t}{\Delta x} \left( \widehat{F}_{i+\frac{1}{2},j}^{(k),n} - \widehat{F}_{i-\frac{1}{2},j}^{(k),n} \right)$ ,  $d\mathcal{M}_{i,j}^{(s),n+1} = d\mathcal{M}_{i,j}^{*(s),n+1}$  and  $f_{i,j}^{(s),n+1}$  is the precomputed value at  $t = t^{n+1}$  for each grid points using classical schemes. From (D.1), we have

$$(D.2) \quad \begin{aligned} & \left( 1 + b_s \frac{\Delta t}{\kappa} \right) \sum_{i=1}^{N_x} \sum_{j=0}^{N_v} \left( f_{i,j}^{n+1} - f_{i,j}^{*n+1} \right) \phi(v_j) \Delta v \Delta x \\ &= \sum_{i=1}^{N_x} \sum_{j=0}^{N_v} \left[ \frac{\Delta t}{\kappa} \sum_{k=1}^{s-1} b_k \left( d\mathcal{M}_{i,j}^{(k),n+1} - f_{i,j}^{(k),n+1} \right) + \frac{\Delta t}{\kappa} b_s \left( d\mathcal{M}_{i,j}^{(s),n+1} - f_{i,j}^{*n+1} \right) \right] \phi(v_j) \Delta v \Delta x. \end{aligned}$$

Using

$$\max_i \left\| \sum_{j=0}^{N_v} \left[ f_{i,j}^{(k),n+1} - d\mathcal{M}_{i,j}^{(k),n+1} \right] \phi(v_j) \Delta v \right\|_{\infty} \leq tol,$$

we can get from (D.2)

$$\begin{aligned} & \left\| \left( 1 + b_s \frac{\Delta t}{\kappa} \right) \sum_{i=1}^{N_x} \sum_{j=0}^{N_v} \left( f_{i,j}^{n+1} - f_{i,j}^{*n+1} \right) \phi(v_j) \Delta v \Delta x \right\|_{\infty} \\ & \leq \frac{\Delta t}{\kappa} \sum_{i=1}^{N_x} \left( \sum_{k=1}^{s-1} |b_k| + |b_s| \right) tol \Delta x \\ &= \left( \sum_{k=1}^{s-1} |b_k| + |b_s| \right) \frac{\Delta t}{\kappa} (x_{max} - x_{min}) tol. \end{aligned}$$

For any dirk scheme of order  $s$ , we have  $b_s > 0$ , which implies

$$\left\| \sum_{i=1}^{N_x} \left( f_{i,j}^{n+1} - f_{i,j}^{*n+1} \right) \phi(v_j) \Delta v \Delta x \right\|_{\infty} \leq \left( \sum_{k=1}^{s-1} |b_k| + |b_s| \right) \frac{\Delta t}{\kappa + b_s \Delta t} (x_{max} - x_{min}) tol.$$

Moreover, the periodic boundary condition gives

$$\sum_{i=1}^{N_x} \sum_{j=0}^{N_v} f_{i,j}^{*n+1} \phi(v_j) \Delta v \Delta x = \sum_{i=1}^{N_x} \sum_{j=0}^{N_v} f_{i,j}^n \phi(v_j) \Delta v \Delta x,$$

and hence

$$\left\| \sum_{i=1}^{N_x} (m_i^{n+1} - m_i^n) \Delta x \right\|_{\infty} \leq \left( \sum_{k=1}^{s-1} |b_k| + |b_s| \right) \frac{\Delta t}{\kappa + b_s \Delta t} (x_{max} - x_{min}) tol.$$

Finally, we can conclude that

$$\begin{aligned} & \left\| \sum_{i=1}^{N_x} (m_i^{N_t} - m_i^0) \Delta x \right\|_{\infty} \leq \sum_{i=1}^{N_x} \sum_{r=1}^{N_t} \left\| (m_i^r - m_i^{r-1}) \Delta x \right\|_{\infty} \\ & \leq \left( \sum_{k=1}^{s-1} |b_k| + |b_s| \right) \frac{N_t \Delta t}{\kappa + b_s \Delta t} (x_{max} - x_{min}) tol. \end{aligned}$$

□

Similar results hold for the BDF methods, which can be derived from similar (but more tedious) argument. We present it without proof.

**Proposition D.2.** *In the periodic boundary condition, conservation error estimates for the BDF scheme of order  $s = 2, 3$  in mass, momentum and energy are given by*

$$(D.3) \quad \begin{aligned} & \left\| \sum_{i=1}^{N_x} (m_i^{N_t} - m_i^0) \Delta x \right\|_{\infty} \\ & \leq \gamma_s \left( \frac{(N_t - s) \beta_s \Delta t}{\kappa + \beta_s \Delta t} + \left( \sum_{k=1}^{s-1} |b_k| + |b_s| \right) \frac{s \Delta t}{\kappa + b_s \Delta t} \right) (x_{\max} - x_{\min}) tol, \end{aligned}$$

where  $b_k$ ,  $k = 1, \dots, s$  and  $\beta_s$  are determined for each  $s = 2, 3$  and  $\gamma_2 = \frac{3}{2}$  and  $\gamma_3 = \frac{146}{11}$ .

## REFERENCES

1. P. Andries, J.-F. Bourgat, P. Le Tallec, and B. Perthame, *Numerical comparison between the Boltzmann and ES-BGK models for rarefied gases*, Comput. Methods Appl. Mech. Engrg. **191** (2002), no. 31, 3369–3390.
2. P. Andries, P. Le Tallec, J.-P. Perlat, and B. Perthame, *The Gaussian-BGK model of Boltzmann equation with small Prandtl number*, Eur. J. Mech. B Fluids **19** (2000), no. 6, 813–830.
3. U. M. Ascher, S. J. Ruuth, and R. J. Spiteri, *Implicit-explicit Runge-Kutta methods for time-dependent partial differential equations*, Appl. Numer. Math. **25** (1997), no. 2-3, 151–167.
4. C. Bardos, F. Golse, and D. Levermore, *Fluid dynamic limits of kinetic equations. I. Formal derivations*, J. Stat. Phys. **63** (1991), no. 1-2, 323–344.
5. P. L. Bhatnagar, E. P. Gross, and M. Krook, *A model for collision processes in gases. Small amplitude process in charged and neutral one-component systems*, Phys. Rev **94** (1954), no. 2, 511–525.
6. F. Bouchut, F. Golse, and M. Pulvirenti, *Kinetic Equations and Asymptotic Theory*, Gauthier-Villars, Paris, 2000.
7. E. Carlini, R. Ferretti, and G. Russo, *A Weighted Essentially Nonoscillatory, Large Time-Step Scheme for Hamilton-Jacobi Equations*, SIAM J. Sci. Comput. **27** (2005), no. 3, 1071–1091.
8. C. Cercignani, *The Boltzmann Equation and Its Applications*, Springer, New York, 1988.
9. S. Chapman and T.G. Cowling, *The Mathematical Theory of Non-Uniform Gases*, 3rd ed., Cambridge University Press, 1970.
10. N. Crouseilles, M. Mehrenberger, and E. Sonnendrcker, *Conservative semi-Lagrangian schemes for Vlasov equations*, J. Comput. Phys. **229** (2010), no. 6, 1927–1953.
11. F. Filbet, E. Sonnendrcker, and P. Bertrand, *Conservative Numerical Schemes for the Vlasov Equation*, J. Comput. Phys. **172** (2001), 166–187.
12. M. Groppi, G. Russo, and G. Stracquadanio, *High order semi-Lagrangian methods for the BGK equation*, Commun. Math. Sci. **14** (2016), no. 2, 389–414.
13. E. Hairer and G. Warner, *Solving Ordinary Differential Equations II: Stiff and Differential-Algebraic Problems*, Springer, Berlin, 1996.
14. E. Hairer, G. Warner, and S. P. Nørsett, *Solving Ordinary Differential Equations I: Nonstiff Problem*, Springer, Berlin, 1996.
15. L. H. Holway, *Kinetic theory of shock structure using and ellipsoidal distribution function in Rarefied Gas Dynamics*, Proceedings of the Fourth International Symposium **1** (1964), 193–215.
16. S. Jin, *Asymptotic preserving (AP) schemes for multiscale kinetic and hyperbolic equations: A review*, Lecture Notes for Summer School on "Methods and Models of Kinetic Theory" (M&MKT), Porto Ercole (Grosseto, Italy), Riv. Math. Univ. Parma **3** (2010), 177–216.
17. L. Mieussens, *Discrete velocity model and implicit scheme for the BGK equation of rarefied gas dynamics*, Math. Models Methods Appl. Sci. **10** (2000), no. 8, 1121–1149.
18. R. M. Pidatella, G. Puppo, G. Russo, and P. Santagati, *Semiconservative finite volume schemes for conservation laws*, SIAM J. Sci. Comput. (submitted).
19. S. Pieraccini and G. Puppo, *Implicit-explicit schemes for BGK kinetic equations*, J. Sci. Comput. **32** (2007), 1–28.
20. J. M. Qiu and C. W. Shu, *Conservative high order semi-Lagrangian finite difference WENO methods for advection in incompressible flow*, J. Sci. Comput. **230** (2011), no. 4, 863–889.
21. G. Russo, J. Qiu, and X. Tao, *Conservative Multi-Dimensional Semi-Lagrangian Finite Difference Scheme: Stability and Applications to the Kinetic and Fluid Simulations*, J. Sci. Comput. (2018), 1–30.
22. G. Russo and P. Santagati, *A new class of large time step methods for the BGK models of the Boltzmann equation*, arXiv:1103.5247 (2011).
23. G. Russo, P. Santagati, and S.-B. Yun, *Convergence of a semi-Lagrangian scheme for the BGK model of the Boltzmann equation*, SIAM J. Numer. Anal. **50** (2012), no. 3, 1111–1135.
24. G. Russo and S.-B. Yun, *Convergence of a semi-Lagrangian scheme for the ellipsoidal BGK model of the Boltzmann equation*, SIAM J. Numer. Anal. **56** (2018), no. 6, 3580–3610.
25. P. Santagati, *High order semi-Lagrangian schemes for the BGK model of the Boltzmann equation*, Department of Mathematics and Computer Science, University of Catania. PhD. thesis, (2007).

26. C. W. Shu, *Essentially non-oscillatory and weighted essentially non-oscillatory schemes for hyperbolic conservation laws*. In *Advanced numerical approximation of nonlinear hyperbolic equations* (Cetraro, 1997), volume 1697 of *Lecture Notes in Math*, Springer, Berlin, 1998.
27. B. Yan and S. Jin, *A successive penalty-based asymptotic-preserving scheme for kinetic equations*, SIAM J. Sci. Comput. **35** (2013), no. 1, A150–A172.

SEBASTIANO BOSCARINO, DEPARTMENT OF MATHEMATICS AND INFORMATICS, UNIVERSITY OF CATANIA, 95125 CATANIA, ITALY

*E-mail address:* boscarino@dmi.unict.it

SEUNGYEON CHO, DEPARTMENT OF MATHEMATICS, SUNGKYUNKWAN UNIVERSITY, SUWON 440-746, REPUBLIC OF KOREA

*E-mail address:* chosy89@skku.edu

GIOVANNI RUSSO, DEPARTMENT OF MATHEMATICS AND INFORMATICS, UNIVERSITY OF CATANIA, 95125 CATANIA, ITALY

*E-mail address:* russo@dmi.unict.it

SEOK-BAE YUN, DEPARTMENT OF MATHEMATICS, SUNGKYUNKWAN UNIVERSITY, SUWON 440-746, REPUBLIC OF KOREA

*E-mail address:* sbyun01@skku.edu